Microfluidic High Throughput Single Cell Mechanotyping: Devices and Applications

Gihoon Choi 1,+, Zifan Tang1, and Weihua Guan 1,2,*

¹ Department of Electrical Engineering, Pennsylvania State University, University Park, PA, 16802, USA

² Department of Biomedical Engineering, Pennsylvania State University, University Park, PA, 16802, USA

* Corresponding Author, Email: w.guan@psu.edu (W. Guan)

⁺ Presently at Department of Biotechnology & Bioengineering, Sandia National Laboratories, Livermore, CA, 94550, USA

Abstract: The mechanical behavior of individual cells plays an important role in regulating various biological

activities at the molecular and cellular levels. It can serve as a promising label-free marker of cells' physiological

states. In the past two decades, several technologies have been developed for understanding the correlations

between cells' mechanical changes and human diseases. However, numerous technical challenges remain

towards realizing high-throughput, robust and easy-to-operate measurements on single-cell mechanical

properties. In this paper, we review the emerging tools enabled by microfluidic technologies for single-cell

mechanical characterization. Different techniques have been benchmarked by considering their advantages and

limitations. Finally, the potential applications related to cell mechanical properties by microfluidic technologies

are discussed.

Keywords: microfluidic; single-cell; cell deformability; mechanotyping.

Article Highlights

Single-cell mechanotyping is an emerging label-free biophysical marker to understand cell states and the

progression of diseases.

Pressurizing, examining, and sorting/separation are three essential functional modules for single-cell

mechanotyping to be translated into biomedical and clinical applications.

Standardization of existing techniques, molecular specificity, high-throughput deformability

characterization, and active-sorting are important future topics for practical implication.

1

1 Introduction

As the basic building block for living organisms, cells can effectively adapt to their microenvironment and respond accordingly by altering their biological, chemical, and physical properties ¹⁻⁴. Among those properties, the mechanical properties of the cell are determined mostly by cellular shells (*e.g.*, plasma membrane), integral structures of the cytoskeleton (*e.g.*, intermediate filaments and microtubules), and the nucleus ^{5,6}. To date, various diseases and biological processes are associated with alternations in cell mechanical properties. Cell mechanical properties have been used as a potential marker for identifying a pathological state. For example, the decrease of red blood cell (RBC) deformability in malaria ⁷ or sickle cell anemia ⁸; the stiffening of white blood cells (WBCs) in sepsis, trauma, and acute respiratory distress syndrome ⁹; the increased cell deformability of invasive cancer cells ¹⁰; and the deformability varication during the stem cell differentiation process ^{6,11,12} can be considered.

To fully exploit the mechanical profiling of cells, detailed measurements with many cells are desirable for statistically significant analysis of cell subpopulations. Current methods for mechanical phenotyping, such as Atomic Force Microscopy (AFM) ¹³⁻¹⁶, micropipette aspiration (MA) ^{17,18}, Optical stretching ¹⁹⁻²², and acoustic actuation ^{23,24}, provide detailed and accurate cell modulus measurements of a small subset of an entire cell population. However, due to the slow detection speeds, the analyzed sample size was typically limited to less than 100 cells/day. By contrast, fluorescence-activated cell sorting (FACS), a commonly used technique for cell characterization, operates at the throughput of up to 10⁴ cells per second and provides the ability for real-time measurement of the cells for sorting purposes.

In this work, recent microfluidic high throughput techniques for single-cell mechanotyping are reviewed and summarized. Single-cell mechanotyping involves three basic function modules: pressurizing (actuation), examining (sensing), and sorting/separation (actuation). We summarized state-of-the-art microfluidic techniques in these areas for high throughput single-cell mechanical study. We benchmarked these techniques based on their working mechanisms and discussed their advantages and rooms for improvements. This was followed by summarizing various applications based on microfluidic cell mechanotyping, ranging from cell separation, disease diagnosis to drug discovery. Finally, we will present perspectives on the opportunities and challenges for further developing and applying microfluidic-based cell mechanotyping.

2 To press

2.1 Physical constriction

One of the cell-stretching strategies in a microfluidic device is to flow the cells into the geometric constriction where the channel walls squeeze a single cell. In this method, the level of cell deformation is mainly determined by the channel geometry, such as width, although the driving force and shape of the constriction edges are also contributing factors ^{25,26}. Therefore, the channel geometry needs to be well-matched with a cell diameter. Typically, the channel width is designed slightly smaller than the cell diameter to ensure cell deformation. However, the predefined channel geometry often limits the analysis of polydisperse samples in size (e.g., whole blood) since channel geometry is not adjustable.

During the past decade, constriction-based microfluidic technology enables high-throughput and precise quantification of the individual cell deformability (**Fig. 1**). The quantification of mechanical properties is achieved by measuring the time-dependent readouts (*i.e.*, transit velocity and transit time), which are often extracted from conductance changes (**Fig. 1(a) and (b)**) ^{10,27-30}, frame streams of optical imaging (**Fig. 1(c)**) ³¹, and pressure drops across the constriction (**Fig. 1(d)**) ³². The most advanced measurement throughput was reported to ~500 cells/s by electrical measurement ⁷. Such measurement rate is significantly higher than the conventional deformability characterization methods, such as AFM, micropipette aspiration, and optical tweezer. Due to its prominent throughput, constriction-methods are particularly useful for deformability measurement of biological samples (*e.g.*, RBCs, leukocytes, cancer cells, and stem cells), where a large number of samples need to be characterized to build reliable statistics. The specific examination techniques (high-speed imaging, electrical measurement, and buoyant mass sensing within resonant cantilever) to indirectly measure time-dependent readouts will be discussed in Section 3.

The time-dependent readouts allow estimating the elastic modulus or stiffness of cells by following power-law rheology ³³,

$$t = \left[\frac{\varepsilon_{max} E}{\Lambda \bar{P}}\right]^{\frac{1}{\beta}}$$

where t, \mathcal{E} , \mathcal{E} , \mathcal{E} , and β are time, strain, elastic modulus, pressure drop across the constriction, and power-law exponent, respectively. A higher β value implies a more viscous behavior while a lower β to a more elastic behavior (Typically, 0.1-0.5 for live cells). For constriction methods, channel

width (w) and height (h) is important design consideration to determine the cell strain (\mathcal{E}) . The following equation describes the max strain when the cell squeeze through the constriction (R_{cell}) denotes the cell radius before deformation)²⁷.

$$\mathcal{E}_{max} = \frac{R_{cell} - R_{eff}}{R_{cell}}$$
 , $R_{eff} = \sqrt{w \times h/\pi}$

Typically, R_{eff} is designed to be smaller than the R_{cell} to ensure the cell deformation at constrictions. Although several existing works suggested R_{eff} be two times smaller than the R_{cell} , the optimal channel width and height are often empirically determined since various factors can affect the measurement, such as driving pressure, fluidic channel wettability, and friction 34 .

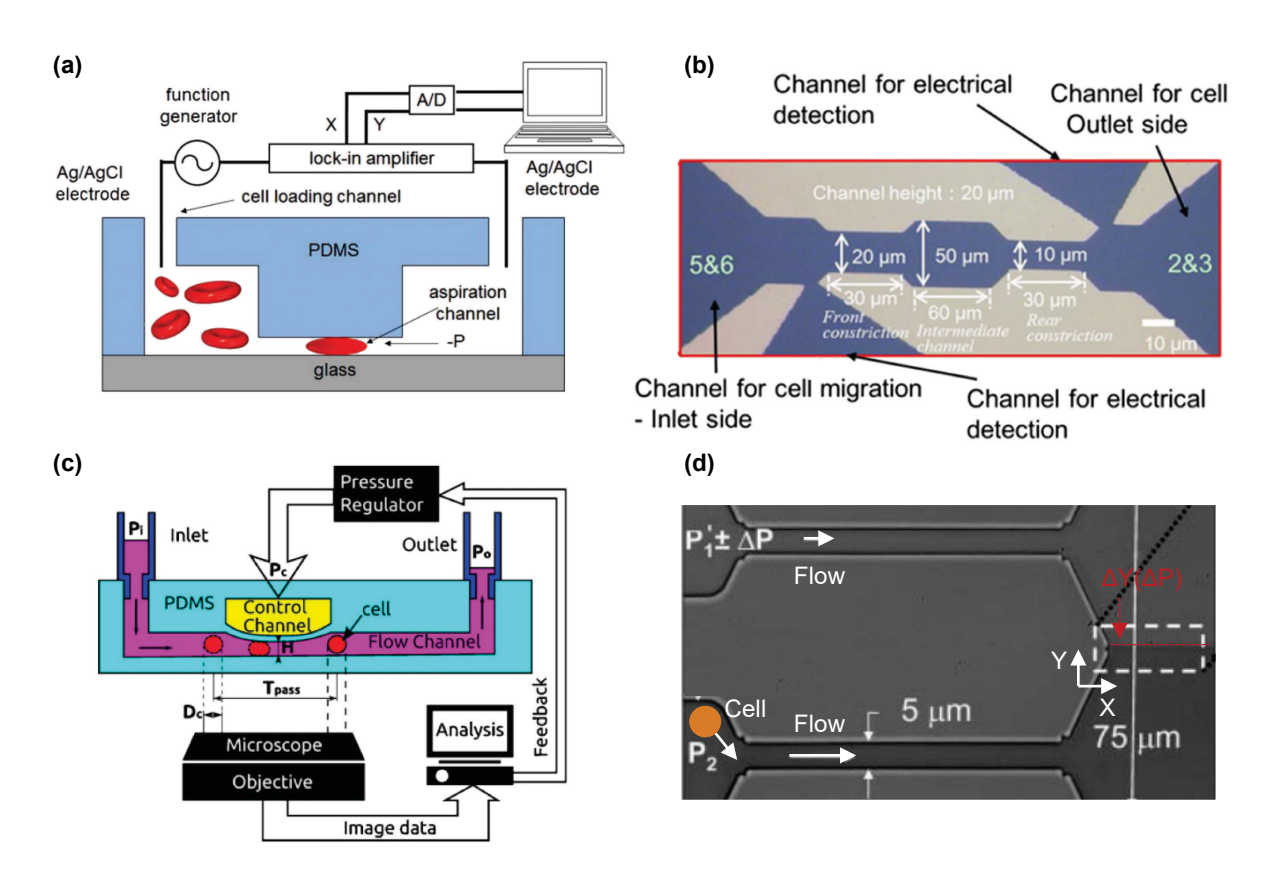


Fig. 1. Physical constriction microfluidic device with various geometries and readouts for cell deformability measurement. (a) The conductance changes were monitored when the cell squeezed through the constriction pore. The width of the signal peak indicates the transit time ²⁸. (b) Two consecutive constrictions with different widths were used for cell size and deformability measurement ³⁰. Transit time was electrically measured. (c) Size-independent deformability cytometry using real-time adjustable constriction ³¹. The system can control the constriction height for polydisperse samples in size. The cell transit velocity (or time) information was extracted from a time-dependent cell position in the microfluidic channel. (d) Microfluidic constriction-based pressure manometer ³². The y-positional change directly indicated the pressure drop across the

constriction during the cell translocation event.

The constriction type can be categorized into single- and multichannel methods. The single-channel constriction method is often challenged to distinguish deformable cells when the cell transit time distributions are closely overlapped with each other. The transit time difference between cells can be amplified to achieve more sensitive differentiation by using a more extended constriction channel. However, a more prolonged constriction is susceptible to irreversible channel blockage. To compromise those two factors, multi-constriction design can be considered. The idea is that each constriction channel length is short enough to avoid clogging, while a series of multiple constriction structures amplify the transit time differences (**Fig. 2(a)**) ³⁵. A sequential constriction array can also be used in a parallel scheme to increase transit time difference and measurement throughput (**Fig. 2(b)**) ^{36,37}.

Similarly, the parallelism of single-constriction was reported to achieve high-throughput measurement at the single-cell level (**Fig. 2(c)**) 27,38,39 . For all parallel constriction methods, bypass channels were commonly used to provide constant pressure drop across the constriction arrays and prevent clogging. Recently, differential micro-constriction arrays were reported to investigate the cell deformation and relaxation process based on the electrical impedance measurement (**Fig. 2(d)**). Successive constrictions provide sensitive transit time information ($T_1+T_2+T_3+T_4$) as well as relaxation index (T_4/T_1) of single cells at a measurement rate higher than 430 cell/min 40 .

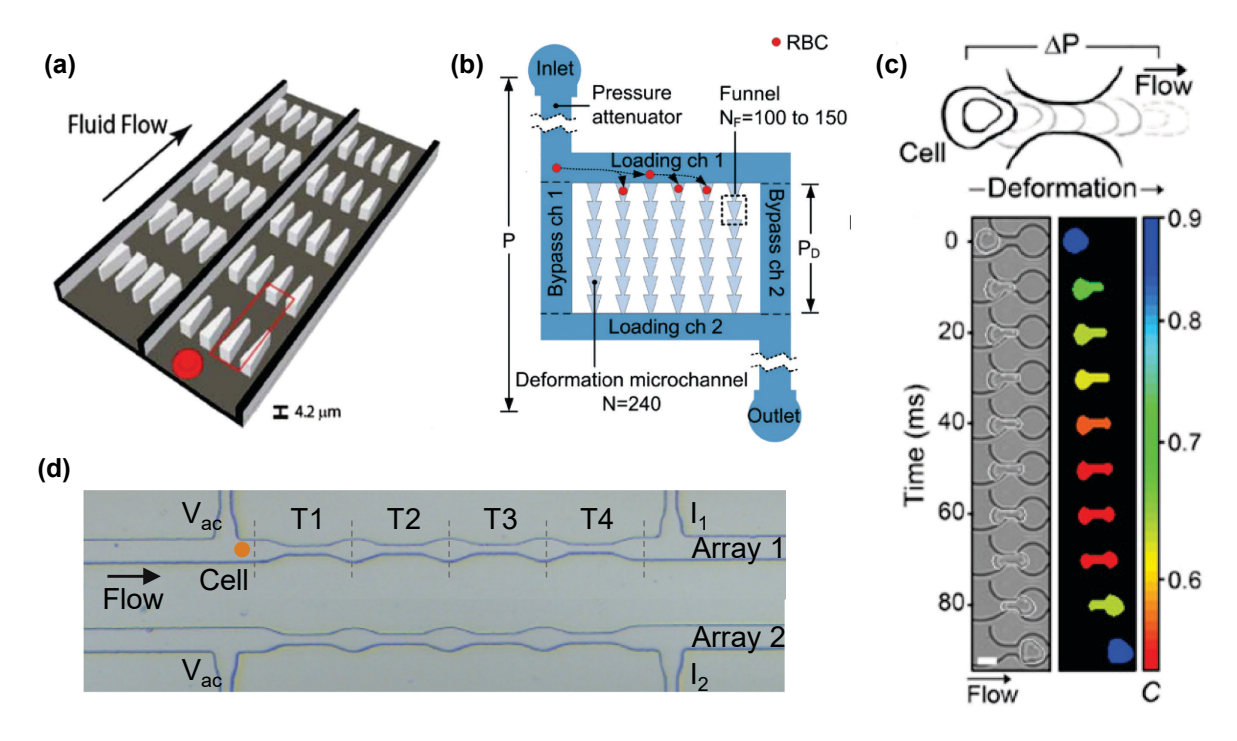


Fig. 2. Various multi-constriction methods. (a) Deformability-based flow cytometry using series constrictions ³⁵. (b) Microfluidic cell-phoresis device using sequential constriction in parallel ³⁷. (c) Quantitative deformability cytometry using parallel constriction array for rapid and calibrated measurement ³⁸. (d) Parallelized differential multi-constrictions in series for cell deformation and relaxation measurement ⁴⁰.

Although the physical constriction method is an excellent technique for high-throughput and sensitive measurement of cell deformability, there is a fundamental limitation to be addressed. As the cell walls were in contact with the channel walls, time-dependent transit velocity (or time)-based deformability measurement was convolved with cell size and surface properties of cells and channel walls ³⁴. To some extent, it is possible to decouple the cell size, using adjustable constriction pores ³¹ and physical constriction integrated with microfluidic Coulter counter (particle size analyzer) ^{29,30}. However, the approach to precisely decouple quantitative mechanical properties from convolved factors still need room for improvement.

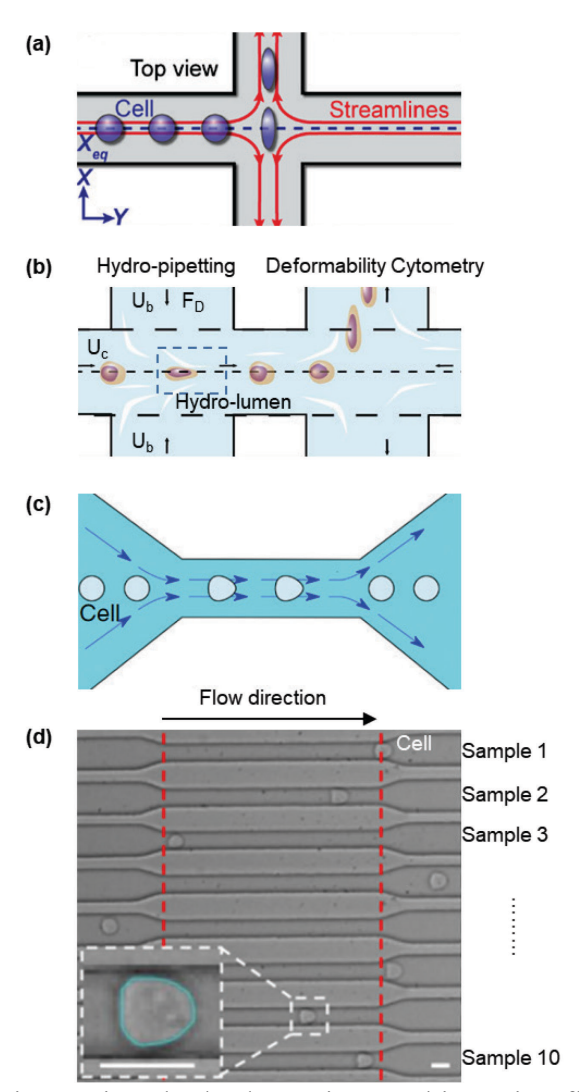


Fig. 3. Cell deformation using various hydrodynamic stretching microfluidic device geometry: (a) Cross-junction ⁴¹, (b) hydro-pipetting with cross-junction ⁴², (c) funnel shape ⁴³, (d) funnel-shaped fluidic channel array ⁴⁴.

2.2 Hydrodynamic stretching

Hydrodynamic approaches measure the mechanical properties of cells by using intrinsic fluid-dynamic stresses that the geometry of the microfluidic channels can tune. While adhesive properties of cells affect deformability measurement in the physical constriction method, contact-free hydrodynamic stretching can decouple this factor and provide direct evidence of cell deformability. Besides, heterogeneous cell size can be independently measured and considered in mechanical models to avoid the misinterpretation of mechanical properties. Although additional upstream cell focusing (*e.g.*, inertial focusing ⁴⁵ and viscoelastic focusing ⁴⁶) is required for the

uniform stress field, the hydrodynamic approach can deform the cell at high rates with sufficient strain (40 - 50%).

The hydrodynamic stress exerted on cells in the microfluidic channel can be categorized into shear and compressive forces depending on the dominant flow regimes ⁴⁷. For example, compressive force is a dominant force for cell deformation in the inertia flow regime (Re>>1), while shear force is dominant in the shear regime (Re<<1). Following equations describe the compressive and shear forces,

$$F_{compress} \cong \frac{1}{2} \rho U^2 C_D A$$

 $F_{shear} \cong 2\pi U \mu r$

where fluid velocity (U), fluid density (ρ), viscosity of suspension media (μ), cross-sectional area of the channel (A), cell radius (r), and drag coefficient (C_D) are adjustable experimental/design parameters to ensure the sufficient cell compression. In addition, the work of Armistead et al.⁴⁷ showed that dominant force should be carefully chosen based on the application since deformability response to the type of applied forces showed different sensitivity despite the same magnitude. For example, the shear-dominant regime showed better sensitivity in monitoring deformation of the cell membrane and the cytoskeleton, while the inertial regime works better for cytosol and nucleus deformation.

In 2012, Dino Di Carlo's group reported a hydrodynamic-stretching microfluidic device for identifying the malignant cell in a human pleural fluid sample with a measurement speed of 2000 cells s⁻¹ ⁴¹. Cells were focused on a narrow streamline near the center of the microfluidic channel and delivered to a cross-junction at a high flow rate, where the cells undergo mechanical stretching by perpendicular crossflows (**Fig. 3(a)**). Cell deformations were captured using a high-speed camera, and images were off-line analyzed to extract the cell volume and deformation index (DI). The throughput of the system was limited when cells could reside at the stagnation point in cross-junction. The following work rectified such limitation by a unique combination of a self-sheathing flow and the pinched-flow, resulting in a significant throughput enhancement (up to 65,000 cells s⁻¹) (**Fig. 3(b)**) ⁴². Recent advancement was achieved by Otto *et al.*, who developed real-time deformability cytometry (RT-DC) (**Fig. 3(c)**) ⁴³. In this system, cells flowed through a funnel-shaped microfluidic channel and were deformed by hydrodynamic stress and pressure gradient. Since the funnel-shaped channel had a width larger than the cell diameter, cells were deformed

without physical contact. The deformability was measured by monitoring cell circularity change in real-time with analysis rates greater than 100 cell s⁻¹. Beyond the deformability characterization, the real-time system provides an excellent potential for label-free single-cell-level cell sorting based on mechanical properties. Besides, the simple funnel-shaped channel structure is easy to scale up for multiplexing. The parallelism of the flow-induced cell deformation was demonstrated by Ahmmed *et al.* by multi-sample deformability cytometry ⁴⁴. The array device consists of 10 funnel-shaped fluidic channels, which simultaneously deforms the cell at a rate of 100 cell s⁻¹ per channel. Therefore, multiple samples can be analyzed in a high-throughput manner (**Fig. 3(d)**).

The aforementioned hydrodynamic approaches have their limitations. In the cross-junction method (Fig. 3(a) and (b)), uneven cell deformation may occur due to the flow instability and intrinsic hydraulic resistance asymmetry displacing the cell off from the stagnation point. A key challenge for the funnel-shaped microchannel approach (Fig. 3(c)) is non-uniformity in the shear stress and hydrodynamic pressure within the microchannel, causing irregular cell deformation forces. To address this problem, the cell must be well-aligned in the center of the channel using burdensome sheath fluids or various hydrodynamic focusing techniques. Finally, the cell size and shape affect the stress field in fluid, acting on a cell for deformation. Therefore, novel approaches to decouple these interfering factors are needed for mechanical property measurements.

2.3 Optical stretching

Another approach to deform a cell is through optical forces. In the past, various optical-based non-contact cell manipulation methods were reported, including an optical tweezer and trap. However, the small magnitude of optically induced force (less than a couple of hundred piconewtons) is insufficient for stiff cell deformation, thus often limits its application in mechanotyping research. To address this problem, the optical stretcher was developed. The first microfluidic optical stretcher was developed by Guck *et al.* to study the deformability of circulating cells (*e.g.*, RBCs and human epithelial breast cancer cells) ¹⁹. The stretching mechanism employed the nano-newton range of light-induced surface force exerted on a cell by two non-focused counterpropagating Gaussian laser beams. While low intensities of laser beams were used to localize the cells, high laser intensities (few milliwatts) were used to stretch the cells along the axis of the beams. The stretching forces were generated by the momentum transfer, which occurred at the interface between the cell and the surrounding medium due to a refractive index change. As

a result, the sufficient surface force stretched the localized cell apart.

The throughput of the optical stretcher has been gradually evolved. In Guck's following work, an optical stretcher was integrated with a microfluidic system, which continuously placed the cells in the trapping and stretching zone ²². Due to automated flow control, the deformability measurement rate of 1 cell/min was achieved. In this system, the rate-limiting factor was mainly determined by the imaging time for observing the small creeping cellular deformation. In 2013, Sawetzki *et al.* also characterized the viscoelastic properties of healthy and malaria-infected RBCs at a measurement rate higher than 20 cells/sec using a high-frequency modulated deformation force ⁴⁸.

Although the throughput of the optical stretcher was higher than conventional AFM, micropipette aspiration (~0.1 cell/min) is still not comparable to the aforementioned microfluidic-based deformability measurement methods such as physical constriction and hydrodynamic stretching. However, the working principle of the optical stretcher is independent of the flow characteristics; thus, it allows characterization of time-dependent mechanical properties of cells such as stress relaxation ^{49,50} and creep indentation ⁵¹. To avoid radiation damage to cells, the laser intensities and wavelength need to be carefully selected.

Table 1. Summary of various microfluidic techniques to compress cells for deformability characterization.

	Channel contact	Critical channel	Channel width × height (μm)	Cell driving	Pressure (kPa)	Cell lines	Deformability measure	Deformation timescale (ms)	Throughput (cell/min)	Ref.
	Contact	8 parallel constrictions	5 × 9	Pressure	0.1 - 0.8	Lukemia breast carcinoma	Transit time	5 - 10	180	27
	Contact	Single constriction	3 × 5	Pressure	3	RBC	Transit time	1 - 3	9×10^{3}	28
	Contact	2 consecutive constrictions	$8 \times 8 \text{ (size)}$ $5 \times 5 \text{ (stiffness)}$	Pressure	0.4 -1.6	RBC	Transit time	10	600	29
	Contact	2 consecutive constrictions	$20 \times 20 \text{ (size)}$ 10×20 (stiffness)	Syringe, Electro- phoresis	0.16	Hela, Jurkat	Transit time	8-23	6×10^{3}	30
	Contact	Single constriction	$50 \times (30 - \alpha)$ (Adjustable)	Pressure	-	RBC	Transit time	500	-	31
Physical Constriction	Contact	Single constriction	5 × 5	Pressure	34.5	RBC & WBC	Pressure change	50	-	32
Physical onstrictio	Contact	Single constriction	5 × 5	Pressure	6.9	Malaria iRBC	Transit time	70 - 150	3×10^{4}	7
F Sign	Contact	Constriction pillars	3 × 4	Pressure	-	Malaria iRBC	Transit velocity	-	120	35
•	Contact	8 parallel array (100 constrictions / array)	2 × 4	Pressure	0.015	Malaria iRBC	Spatial distribution	-	-	37
	Contact	16 parallel arrays	5 × 10 (HL60) 9 × 10 (MCF7, MDA-MB-231)	Pressure	28	HL60, MCF7, MDA-MB-231	Transit time	7.5 - 200	1×10^{3}	38
	Contact	64 parallel capillary- like microchannel	6 × 13	Pressure	0.01-1	RBC, HL60	Transit time	200 - 600	120	39
	Contact	2 parallel array (4 constrictions / array)	10 × 20	Pressure	50	MCF7	Transit time	5 -10	430	40
	Contact	16 parallel array (6 constrictions / array)	5 × 5	Pressure	28	HL60	Transit time	10 - 100	100	34
	Contact-free	Cross-junction	60 × 30	Syringe pump	-	MCF7	Aspect ratio	0.01	1.2×10^{5}	41
ıamic ing	Contact-free	Cross-junction	100 × 30	Syringe pump	-	Hela, Jurkat, MCF7	Aspect ratio	0.01	3.9×10^{6}	42
Hydrodynamic Stretching	Contact-free	Funnel-shaped channel	20 × 20	Syringe pump	-	HL60, HSC, Whole blood	Circularity	1	6×10^{3}	43
Hyd St	Contact-free	Funnel-shaped linear channel array	18 × 20	Pressure	15	MCF10A&7, PC3, HMS50, MDA-MB-231& 468, HCC1419	Circularity	2	6 × 10 ⁴	44
Optical Stretching	Contact-free	Linear optical trap	1000 × 10	-	-	Malaria iRBC	Aspect ratio	20	1.2×10^{3}	48
	Contact-free	Linear optical trap	20 × 200	-	-	RBC & WBC	Aspect ratio	25	6×10^{3}	52

3 To examine

3.1 Imaging (endpoint analysis)

Perhaps the most intuitive method to examine the cell deformability is by measuring the changes in a cellular shape corresponding to the applied force on cells (**Fig. 4(a)**). The cellular deformation was quantified by measuring the DI or stretch ratio (e.g., cell circularity and aspect ratio) using high-resolution imaging ^{41,42,53-55}. One of the key benefits of the imaging method is the direct observation of cell motion, providing cell deformability and the dynamic behavior of the cell. For example, Forsyth *et al.* observed three different types of RBC deformation dynamic motions in microfluidic funnel-shaped capillary at a different shear rate: stretching, tumbling and recoiling using a high-speed imaging camera ^{54,56}. For the characterization of the RBCs' membrane viscoelastic properties, Tomaiuolo *et al.* measured the circularity change induced by the converging/diverging flow in multichannel microfluidic devices ⁵⁷.

Another imaging-based characterization was achieved by measuring the quantitative parameters (*e.g.*, transit time, transit velocity, and entry time) as an indirect indicator of cell deformability when the cell squeezes through the physical constriction (**Fig. 4(b)**). In this case, a time-dependent cell position and its corresponding timestamp were monitored using a high-resolution camera. The less deformable cells spent more time squeezing through the microconstriction than more deformable ones. For instance, Hou *et al.* investigated the bioreheological behavior of breast cancer cells in micro-scale constriction ⁵⁸. In this study, nonmalignant and malignant cells were distinguished by quantitative measurement of entry time, transit velocity, and elongation index from video images.

Several concerns of imaging method have been reported: i) high-resolution image-recording setup is expensive, ii) well-controlled hydrodynamic cell manipulation (*e.g.*, focusing and spacing) is required to locate the cell at the focal spot, and iii) post-image analysis is a time-consuming process and requires massive image data storage and computational power, limiting the actual throughput (*i.e.*, from sample loading to completion of deformability analysis). For the real-world application, the development of deformability flow cytometry has been changed from endpoint to real-time analysis.

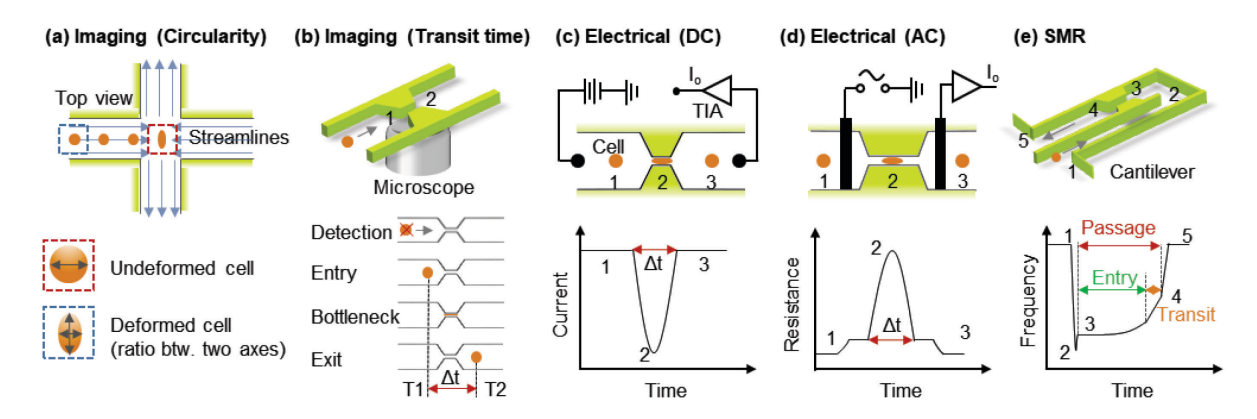


Fig. 4. Schematics of various deformability measurement methods. (a) deformability was measured by the aspect ratio changes of the cell using image processing. (b) cell position and time are extracted by image analysis, yielding the transit time (indirect deformability indicator) of cell translocation at a funnel-shaped constriction channel. (c) DC sensing was used to obtain the ionic current dips, providing cell transit time. (d) The AC measurement monitored resistance/impedance change to obtain the transit time. (e) Mechanical cantilever measures the buoyant forces and their resonant frequency. The transit time, entry time, and passage time can be extracted from the resonant frequency profile.

3.2 Electrical measurement

In constriction-based deformability characterization (see Section 2.1), indirect quantitative parameters for cell deformability are often measured by electrical readouts. The transient changes in electrical current are induced by channel blockage during the cell translocation since current disruption occurs due to the reduced conduction at the physical constriction.

Among various deformability characterization methods, electrical measurement offers the following benefits; i) high-throughput, ii) simplicity, iii) automation, and iv) biocompatibility. However, cell transit time is a complex function of various parameters: the applied pressure, the cell size, the cell deformability, the constriction channel dimensions, and the PDMS and cell surface properties ^{34,59}. Therefore, precise time-dependent readouts are often required with well-defined control parameters to distinguish cell deformability from convolved parameters. As an effort to resolve the cell deformability from the size, Sano *et al.* used two consecutive constrictions with different channel widths to measure size and deformability during translocation events ³⁰.

Fig. 4(c & d) depicts the simplest two-electrode sensing design. Both schemes measure the impedance changes during the cell translocation event by an impedance analyzer (*e.g.*, transimpedance amplifier, lock-in amplifier). An early-stage microfluidics-based impedance sensor for electrical classification of single RBC deformability was devised by Katsumoto *et al.* ⁶⁰. A

microfluidic chip with channels integrated with a pair of coplanar microelectrodes was used to measure the normalized resistance changes, corresponding to the shape of cell deformation in high-shear microchannel flows. Due to the positional dependence of the AC measurement, the obtained amplitude could vary based on the z-dimensional location of the cell from the electrode surface. To enhance the measurement accuracy, a physical constriction channel with electrical sensing has been proposed. For example, Adamo *et al.* demonstrated the dependence of transit time, size, and stiffness of the HeLa cell by monitoring the resistance changes ⁶¹. A similar method was achieved by Zheng *et al.* to compare the biophysical properties of adult RBCs and neonatal RBCs using electrical signatures (*i.e.*, transit time, impedance amplitude, and phase) ²⁸. For the optimal AC measurement, the frequency range of 10 to 200 kHz is typically recommended to compromise the time resolution, the double-layer capacitance, and sensitivity. Electrochemical degradation of the electrode is a significant problem for long-term electrical measurement since it causes baseline shift, lower SNR, and lower sensitivity. A key benefit of using AC voltage is suppressing electrode polarization, resulting in reducing electrode degradation and the air bubbles in a microfluidic channel.

3.3 Mechanical measurement using cantilever

The first suspended microchannel resonator (SMR) was developed for biomolecular detection by T.P. Burg and S.R. Manalis ⁶². SMR contains a microfluidic channel embedded in a silicon cantilever. When biomolecules pass through the microfluidic channel, their buoyant mass changes the resonance frequency of the cantilever. Using this principle, the SMR was used for biomolecule detection ⁶³ and buoyant mass, density, volume measurement of a single cell ⁶⁴⁻⁶⁶. In 2013, the SMR technique was applied for characterizing cell deformability and surface friction ¹⁰. Unlike the previously reported SMR, the physical constriction was added in the embedded microfluidic channel to deform the cells. By monitoring the resonance frequency shift, cell entry, transit, and total passage time were extracted to indirectly characterize the cell deformability (**Fig. 4(e)**). The physical contact of cells with constriction channels make SMR stand out for the studies where cell friction or retention is of interest ⁶⁷. The resonant cantilever is extremely sensitive microdevice, which can measure the center of mass and buoyant mass with a precision of 100 nm and 1 pg respectively. However, multi-steps of wafer thinning and dry etching process for microfluidic-channel embedded cantilevers added the fabrication complexity. In addition, untransparent

channel limits the optic-integrated microfluidic system for co-measurement.

3.4 Real-time measurement

The time-dependent cell deformability measurement is often required to acquire data at a high sampling/frame rate (10⁵ samples/s) ⁴¹. While a high sampling rate produces excellent time resolution for monitoring cell deformation, it generates a massive amount of data for burdensome off-line analysis, consuming tremendous computational time. Therefore, the true meaning of throughput with considering deformability analysis is much less (~10 cells/sec) than the reported measurement throughput. To address this limitation, the need for real-time deformability measurement has been recognized.

On-the-fly cell deformability measurement was first reported in RT-DC in 2015 ⁴³. They used an online image analysis algorithm that continuously acquires images from the high-speed CMOS camera at 2,000-4,000 frames/sec and quantifies the DI and size (cross-sectional area). The real-time analysis significantly reduces the memory space needed for image recording and computational cost, enabling high-throughput cell deformability characterization (several hundreds of cells per second). A similar imaging-based real-time approach at an even higher frame rate (100,000 frames/sec) was applied in an inertial microfluidic cell stretcher (iMCS), proving its ability to process an unlimited amount of data ⁶⁸. The first real-time electrical measurement was achieved using differential impedance measurement at a sampling rate of 1MHz ⁶⁹. The cell passage time at constriction was extracted from the electrical signal using a simple peak detection algorithm, which reduces the computational complexity of real-time measurement. This offers a great potential for label-free real-time deformability-activated single-cell sorting ^{70,71}.

Table 2 Summary of the representative microfluidic deformability characterization devices.

	DC		iMCS	SMR	Deformability Sensor	
Cell compression	Hydrodynamic Stretching	Hydrodynamic Stretching	Collision Constriction		Constriction	
Deformability Index	Aspect ratio	atio Circularity Aspect ratio (Passage		(Passage time)-1	Transit time	
Readout	Imaging	Imaging	Imaging	Resonant Frequency	Electrical Resistance	
Analysis	Offline	Real-time	Real-time	Offline	Offline	
Throughput (cell/s)	2,000 - 65,000	100	450	1	500	
Physical contact	No	No	Yes	Yes	Yes	
Ref.	41,42	43,72	68	10	7	

4 To sort

4.1 Collective cell separation

Specific cell types and states often exist with other components that are not of interest. Obviously, in a heterogeneous cell population, different sub-populations will have different biophysical and biomechanical characteristics, resulting in the biased analysis ⁷³. This is valid for mechanotyping research, which investigates cell mechanics to study the functional changes in cells during pathological alteration/metastasis and physiological cellular process (*e.g.*, differentiation, proliferation, and motility). Therefore, a preparative cell separation step based on biophysical properties is required to examine the sub-populations individually.

In recent years, numerous label-free microfluidic approaches have been developed to facilitate a qualitative way of passive separation, which does not rely on any external forces based on mechanical properties. These passive techniques commonly attribute to the high-throughput separation of sub-populations in continuous flow. However, other performance metrics (*i.e.*, recovery rate, purity, enrichment, and efficiency) varies depending on the different separation mechanism; microfiltration, deterministic lateral displacement (DLD), compression ridges, crossflow ratchets, and inertial microfluidics (**Fig. 5**). Although many label-free microfluidic techniques separate the sub-population based on biophysical properties (*i.e.*, size, density, electric polarizability, adhesion, and cell contents) ⁷⁴, we only focus on the deformability-based separation in this review.

4.1.1 Microfiltration

Microfiltration is perhaps the most straightforward and intuitive approach to separate microand nanoscale cells based on their size and stiffness. Microfabricated porous membranes ⁷⁵⁻⁷⁸, micropillars ⁷⁸⁻⁸⁰, and weirs ^{78,81} are extensively used as a filter. Typically, the pore size of the filter is designed close to the cell size to achieve high particle capture efficiency. There are two types of microfiltration methods: dead-end ^{77,82,83} and crossflow filtration ^{75,76}. Briefly, the flow direction is facing the dead-end filter plane, whereas the flow direction is parallel to the filter plane in crossflow. The dead-end approach effectively filters large and stiff cells while it is prone to clogging, which reduced the selectivity of the process. In crossflow filtration, additional sheath flow pushes the cells toward the filter, while crossflow continuously flushes away large and stiff cells captured at the filter interface (**Fig. 5(a)**). Therefore, a unique combination of sheath and crossflow enhances purity and throughput by reducing clogging risk. In order to achieve optimal separation performance, the selection of sheath flow and crossflow is critical. For example, excessive crossflow rate will decrease the chance of filtration, resulting in reduced separation purity ⁸⁴. On the contrary, de-clogging is less effective with extremely low crossflow, leading to a reduced recovery rate ^{75,78}. Although various microfluidic filtration methods were reported ^{74,85}, none of them simultaneously satisfies high recovery efficiency, purity, and throughput. Besides, sample loss and clogging are the inherent challenges to be addressed.

4.1.2 Deterministic Lateral Displacement (DLD)

DLD is another well-established passive separation technique that has been extensively explored over the decade. The first DLD was introduced by Huang et al. in 2004 86. Although early-stage DLD only focused on size-based separation ⁸⁷, additional sorting targets such as deformability, shape, and internal viscosity have gained interest 87-90. In 2014, Holmes et al., for the first time, confirmed a direct correlation between cell stiffness and lateral displacement in a DLD device 91. The deformability-based separation mechanism relies on the structure and geometry of the obstacle array, which determines the laminar flow fields (Fig. 5(b)) 90,91. In principle, indefinitely small-sized non-deformable particles never switch to another streamline without external force. However, deformable particles of finite size can move to the other laminar flow streams because hydrodynamic radius (or stretched size) of deformable cells decreases between the micropillars where the shear stress is greatest. Since the row of micropillars repeats with a certain distance, the streamline position is relative to the array change. Therefore, the relative cell position is also gradually displaced based on its deformability as they pass through each row of the pillars (Fig. 5(b)) 90. The high-resolution of the cell separation depends on the degree of cell deformation, which can be adjusted by pillar geometry (i.e., the shape of a pillar, gap between pillar, number of the iteration of the array) and fluid stresses 87,92-94. A recent study demonstrated that a sharp-edge pillar structure (i.e., diamond and triangular) is more useful to deform the cells by strong bending around the post; thus, the sensitivity of the DLD device can be significantly enhanced ⁹⁴. A high flow rate induces strong shear stress to deform cells; thus, a distinct separation of deformable cells can be obtained 87,92,93. Therefore, it is essential to select the optimal separation parameters according to cell types and downstream applications. With

significant efforts, the current deformability-based DLD device achieved excellent purity (>90%) with a reasonable separation rate (\sim 10⁶ cells/hr) ⁹⁰. However, clogging due to the fouling at post structures and channel surface requires special attention for robust separation.

4.1.3 Compression ridges

Continuous and non-destructive cell separation can be achieved using a periodic diagonal ridge array attached to the top wall of the fluidic channel (Fig. 5(c)) 95. The gap between the diagonal ridge and fluidic channel bottom forms the geometric constriction to compress the cells as they squeeze through periodically. The cell separation trajectory was determined by the interaction between the hydrodynamic drag force and stiffness-dependent elastic deformation force, opposing transverse directions 85,96. While hydrodynamic force is dependent on the secondary circulatory flow, the elastic force is a function of cell stiffness. As a result, cell trajectory gradually diverges at elastic and hydrodynamic equilibrium ⁹⁷. The construction height can adjust the stiffnessdependent elastic force since it determines the degree of cell deformation. Therefore, constriction height is a critical parameter to increase the displacement in the transverse direction, thus enhancing separation resolution. Flow rate is another separation parameter, directly affecting the hydrodynamic force imposed on cells. It was experimentally validated that the flow rate was not a significant contributor to distinct separation ⁹⁶. The ridge width was usually set close to the cell diameter. While small width produces insufficient elastic force for successful separation, large width has a high chance of unwanted cell adhesion and irreversible clogging. The ridge angle is typically designed to 45 degrees to the channel axis since maximum hydrodynamic force can be induced for optimal separation effect 85,96. Ridge spacing is a control parameter for cell relaxation, which can be used to observe cell viscoelastic behavior 98. The diagonal compression ridge accommodates the high degree of cell deformation to enhance the separation effects, especially purity (99%) and throughput (250 cells/sec) ⁹⁶. Another key attribute of this separation technique is a less sensitive nature against the cell size variation ⁹⁶.

4.1.4 Resettable Cell Traps (RCT)

Channel clogging is a significant challenge for most passive separation methods. Several a tunable microfluidic-based approach has been reported to address clogging ⁹⁹⁻¹⁰². The idea is to periodically clear the microfluidic channel before blockage by expanding the channel height using

active pneumatic pressure control. Besides, tunable height enables the ability to precisely control the degree of cell deformation; thus, the selectivity of separation can be adjusted for different samples. Huang *et al.* achieved the proof-of-concept tunable microfilter in 2009 ¹⁰⁰. The tunable filter/trap was integrated with conventional dead-end membrane microfiltration methods. Various configurations of valve actuation and flow operation enable size-dependent selective separation of cells with high separation efficiency (82-89%) at a reasonable filtration rate (3.3-14.9 µl/min). A similar tunable approach was used in a resettable cell trap (RCT) mechanism introduced by Qin *et al.* ¹⁰² and Beattie *et al.* ¹⁰¹. The RCT device used cell traps and flexible diaphragm to achieve the size- and deformability-based separation (**Fig. 5(d)**).

The diaphragm was periodically closed (constricted) and opened (relaxed) the main flow channel by pneumatic control (**Fig. 5(d)**) ¹⁰². When the diaphragm was closed, large and stiff cells were captured in traps while small and soft cells transit through the constriction. The diaphragm was periodically opened to clear the flow channel to prevent clogging and fouling. RCT device had the center and side fins, which strongly support the channel structure when the diaphragm was inflated. Therefore, a well-controlled rectangular channel and rectangular aperture were formed (**Fig. 5(d)**). Such a structure offered improved separation performance in sensitivity and selectivity compared to the previous tunable microfilter ¹⁰⁰. Besides, 3-stage trapping/filtration significantly enhanced the sample enrichment (183-fold) and yield (93.8%). The parallelism of the RCTs enables the separation rate (~15,000 cells/min) ¹⁰². Furthermore, clogging-free passive separation is a strong attribute of RCTs. However, the separation marker for the filtration is a combination of cell size and deformability, limiting the applications where the separation must solely rely on cell deformability.

4.1.5 Microfluidic ratchets

Guo *et al.* first explored the microscale deformability-based ratchet mechanism in 2011 ¹⁰³. In this work, cell deformability was coupled with a local asymmetry to induce an irreversible ratchet mechanism. The unidirectional cell transport suggests selective cell separation based on deformability ¹⁰³. In the following work, the microfluidic ratchet device for high-throughput deformability-based cell separation was demonstrated ¹⁰⁴ and used for phenotypic separation of various samples (*e.g.*, Leukocytes, cancer cells, and malaria-infected RBCs) ¹⁰⁵⁻¹⁰⁸. The separation mechanism used funnel-shaped constriction arrays, whose width was designed larger than the cell

diameter while the exit side was smaller ¹⁰⁴. This structure only allows small and deformable cells to ratchet through the tapered constrictions, while large and stiff ones were blocked. The size of the funnel opening gradually decreases from the bottom row (sample inlet side) to the top row (collection outlet side) (**Fig. 5(e)**). Therefore, a particular diagonal trajectory was formed by oscillatory flow (*i.e.*, clogging and de-clogging flow), which propels the cell population ¹⁰⁶. The captured cells were unclogged by subsequent reverse de-clogging flow and flushed out toward the designated collection outlet by crossflow (**Fig. 5(e)**). Reverse flow approach has been used in microfiltration to address the clogging. However, the reverse flow often pushed back the initially separated cells, resulting in low filter selectivity ¹⁰⁴. In microfluidic ratchets, compressing cells through the tapered constriction along the direction of the funnel requires a less threshold pressure than the opposite direction ^{74,104}. Such physical asymmetry with oscillatory flows only allows unidirectional and irreversible cell transport for selective cell separation. Most advanced microfluidic ratchet-based separation stands out in terms of separation rate (0.5×10⁶ cells/hr), purity (98%), and enrichment (10⁴-fold) ¹⁰⁵⁻¹⁰⁷. Besides, the irreversible cell transport enables excellent selectivity and scalability with a low risk of clogging.

4.1.6 Inertial microfluidics

Various inertial microfluidic techniques for particle/cell manipulation, mostly particle focusing, were first explored by Di Carlo *et al.* in 2007 ⁴⁵. In the following work, the inertial microfluidic separation was achieved by adjusting the particle focusing position based on the particle size ¹⁰⁹. The first deformability-based separation using inertial microfluidic was introduced by Hur *et al.* in 2011 ¹¹⁰. In confined flow, the lateral migration of particles can be induced by the effect of inertial life force, which is a function of particle Reynolds number ^{74,110}. Since particle Reynold number differs by intrinsic characteristics, the particle with different deformability has a distinct inertial focusing position in the fluidic channel. Hur *et al.* used this lateral migration phenomenon in a straight microfluidic channel to separate the deformable particles without external forces ¹¹⁰. There are additional lift forces for the deformable particles, such as viscoelasticity-induced force, dependent on particle size and rigidity. The balance between deformability-induced lift force and inertial lift force determines the equilibrium position in the channel. Therefore, these lateral equilibrium position differences were used to separate and collect particles based on their deformability. For example, more deformable particles moved away from

channel walls due to extra viscoelasticity-induced force. In contrast, stiffer particles were positioned near the channel wall due to the dominant inertial lift force (**Fig. 5(f)**). Recently, Guzniczak *et al.* used a spiral microchannel to add curvature that accelerates the deformable particle displacement and significantly reduces the travel distance compared to the straight microchannel and significantly improves the separation throughput (~3×10⁶ cells/min) ¹¹¹. The inertial microfluidic sorter can achieve high throughput for large-scale enrichment without any microfiltration. Thus, clogging is no longer a concern.

4.2 Active single-cell sorting

In passive sorting, sorting boundaries cannot be adjusted during the experiment since flow geometries were predetermined based on intrinsic cell mechanical properties. This often limits the comparison experiment that requires a sorting condition to be varied within the same device. Besides, the individual particle's quantitative deformability information is inaccessible with passive sorting. The deformability-based active sorting is an attractive option to resolve such limitations. However, surprisingly, only a few existing works demonstrated streamlined active single-cell/particle sorting capability with deformability characterization.

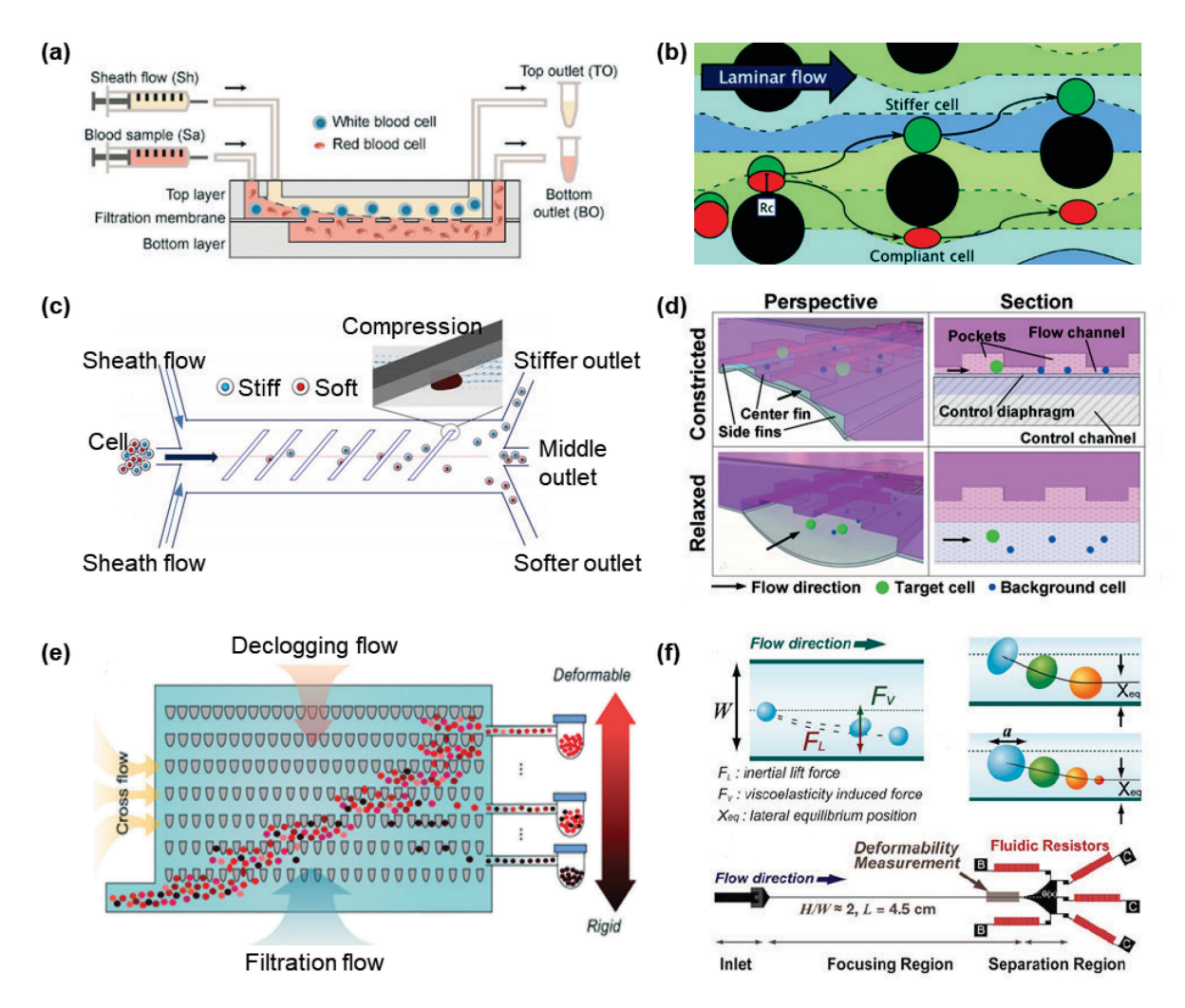


Fig. 5. Various label-free, continuous, and passive bulk cell separation based on cell deformability: (a) porous membrane microfiltration using crossflow ⁷⁵. While larger and stiffer white blood cells are captured at the filter entrance, small and softer red blood cells pass through the filter. (b) deterministic lateral displacement 90. Repeated laminar flow fields were depicted with a circular post array. Stiffer cells shift the streamlines as they pass through the post array while soft cells are deformed and remained in the original streamline. (c) diagonal compression ridge 95. Soft cells are displaced in a negative transverse direction from the channel axis, while ridge cells while stiff ones are moving in the positive transverse direction. Two sheath flows aligned the cells at the channel axis. (d) resettable cell traps ¹⁰². The constricted diaphragm forms the traps to capture the cells of interest, while unwanted cells flow through the traps and collected in the waste outlet. Relaxed diaphragm enlarged the channel dimension to clear the microchannel. (e) microfluidic ratchetsorter 106. Continuous deformability-based cell separation using oscillatory flow and tapered contractions. The more deformable cells travel further up than stiffer ones. Crossflow propels the cells in the horizontal direction toward the collection outlets. (f) inertial microfluidics ¹¹⁰. Inertial lift force (F_L) and viscoelasticity induced force (F_V) are counter-interacted, determining the effective cell position in the channel. The deformable cells tend to stay in the center of the channel axis, while stiff cells move toward the channel walls.

The first active single-cell sorting was reported by Faigle et al. in 2015 112. The optofluidic device was integrated with an optical stretcher to trap, examine, and sort individual cells in sequence (Fig. 6(a)). Counterpropagating two gaussian laser beams were used to real-time measure the single-cell compliance as an indicator of deformability (see Section 2.3). For the sorting mechanism, asymmetric laser profiles were used to displace the cells from the center axis of the fluidic channel toward the desired collection chamber. Unlike the passive bulk cell separation, the throughput of the active sorting system is affected by both sensing and sorting rates. The slow process of optical-based deformability sensing is an inherent rate-limiting factor for fast sorting in the continuous flow. To address the throughput challenge, sorting Real-Time Fluorescence Deformability Cytometry (soRT-FDC) (Fig. 6(b)) was devised 70. The system combined the previously reported real-time fluorescence and deformability cytometry (RT-FDC) ⁷² and downstream standing surface acoustic wave (SSAW)-based active cell sorter ¹¹³. Compared to the optofluidic sorter (Fig. 6(a)), soRT-FDC significantly improved the sorting throughput (100 cells/s) by exploiting the hydrodynamic stretching for rapid deformability characterization. However, high SSAW power for fast cell deflection may cause overheating and degrade the chip integrity and cell viability.

Choi *et al.* developed cytometry-like deformability activated the sorting device ⁷¹. The device seamlessly integrated the single-particle deformability sensing and subsequent active hydrodynamic sorting into a single microfluidic chip (**Fig. 6(c)**). By adapting the fast constriction-based real-time deformability sensing, the system throughput was improved. However, relaxation time, which is the intrinsic limitation of hydrodynamic sorting, still slows down the sorting process. Besides, it often causes incorrect sorting by missing the sorting timing. Li et al. reported phenotyping-activated cell sorting, which integrates real-time electrical impedance measurement with acoustic sorting ¹¹⁴. The impedance measurement can be used to probe cell transit time at constriction for characterizing cell deformability. Besides, sensing electrodes can be configured to determine cell viability by measuring the cell impedance. Propagation of traveling surface acoustic wave (TSAW) generates radiation force and acoustic streaming flow-induced drag force on spherical cells, enabling fast active sorting. Like other deformability-activated single cells/particle sorting techniques, upstream flow cell alignment and well-defined cell spacing will further increase the sorting performance.

Just as Fluorescence-Activated Cell Sorting (FACS) allowed identifying the molecular

characteristics of a leukocyte subpopulation based on immunophenotypes ^{115,116}, mechanotyping based sorting technology will offer a unique opportunity to understand the molecular underpinnings of cell mechanics. To this end, throughput comparable to FACS (30,000 – 40,000 cells/s) and a reliable device that actively sorts large populations of cells one by one based on their mechanical phenotype is urgently needed.

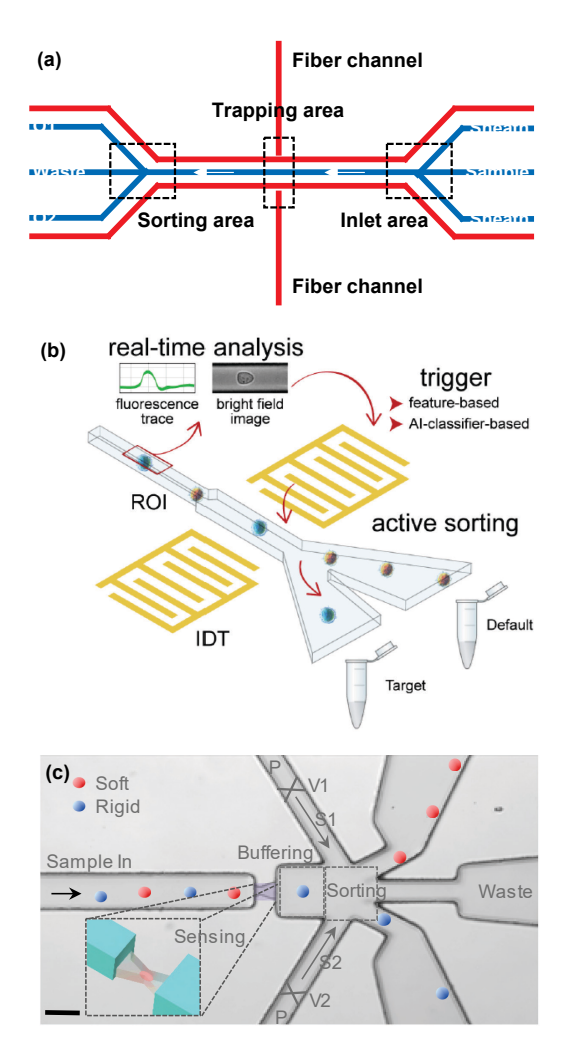


Fig. 6. Various active sorting approaches for a single cell or particle. (a) Optical stretcher integrated with optofluidic sorter ¹¹². Blue channels depict the fluidic channels. Red channels indicate the optical channels. Index matching fluid was filled in the red optical channels. (b) soRT-FDC ⁷⁰. RT-FDC was integrated with a downstream standing surface acoustic wave (SSAW)-based active cell sorter. Three-channel fluorescence imaging was integrated for specificity. (c) Deformability-activated microfluidic particle sorting device ⁷¹. Constriction-based deformability sensor real-time extracts the cell transit time, which was used as a sorting trigger. After deformability measurement, the hydrodynamic sorting mechanism deflects the particle toward the designated collection outlet.

Table 3. Summary of the microfluidic deformability-based cell sorting devices.

	Micro- filtration	DLD*	Compression ridges	RCT*	Ratchets	Inertial	Opto- fluidics	Acousto- fluidics	Hydro- dynamics
Separation type	Bulk	Bulk	Bulk	Bulk	Bulk	Bulk	Active	Active	Active
Separation mechanism	size exclusion	streamline around micro-post array	cell compression	trapping	Irreversible ratchet mechanism	lift forces, secondary flows	optical force (refractive index difference)	acoustic radiation force	Hydro- dynamic push-pull
Separation criteria	size, deformability	size, deformability	size, deformability	size, deformability	size, deformability	size, deformability	deform -ability	deform -ability	Deform -ability
Throughput (cells/min)	10^{4}	10^{7}	10^{4}	10 ⁵	10^{3}	10^{6}	1	10^{3}	600
Purity (%)	80 - 99	90 - 98	65 - 99	-	62 - 95	80	73 - 75	50.3 - 91.3	~ 88
Enrichment (fold)	140 - 232	-	185	183 - 1800	210	100 - 300	~3	~10	~8
Ref.	76,83,117	91	95,96	99,101,102	105-108	74,110	112	70,114	71

DLD: deterministic lateral displacement RCT: resettable cell trapping

5 Applications

5.1 Erythrocytes

Red blood cells (RBCs) or erythrocytes have unique deformability, which allows a reversible change in shape under external forces. This mechanical property plays a critical role in circulating RBCs by carrying oxygen and carbon dioxide through the microvessels and fenestrated capillaries of the splenic sinusoids ¹¹⁸. It has been realized that cell deformability can be altered under various pathophysiological conditions ¹¹⁹. Thus, measuring the RBC deformability can be a valuable indicator to understand hematologic diseases and their progression.

In recent years, various microfluidic techniques have been established to measure RBC deformability, which provides a different aspect of approaches to hematologic diseases. For example, extensive research has been conducted on malaria by investigating hematological abnormalities. The RBC stiffness increases more than 10-fold when the Plasmodium falciparum parasite is infected ^{35,59,120-122}. This mechanical change is causing the occlusions in the peripheral capillaries and spleen ¹²³, disturbing the oxygen transport to the downstream organs and tissues and leading to necrosis. Similarly, the change of RBC deformability has been found in other blood-related diseases such as sickle cell, sepsis, and diabetes ^{124,125}.

Such realization naturally extends to the therapeutic benefits, which the microfluidic separation of diseased RBCs or pathologically activated white blood cells (WBCs) can offers. Unadulterated healthy blood cells can be reintroduced to the patient, while abnormal cells are eliminated by microfluidic separation based on cell mechanics. Such dialysis-like therapeutic approaches ¹²⁶ removes overly activated immune cells such as neutrophils ¹²⁷, malignant bone marrow cells after autologous transplantations ¹²⁸, stiffer malaria-infected cells, and sickle RBCs during a sickle-cell crisis ¹²⁹.

5.2 Stem cells

Over the past decades, extensive effort has been made to reveal how the mechanical properties of stem cells affect pluripotency and differentiation ¹³⁰. During the stem cell differentiation process, gene expression and protein abundance changes modify the cytoskeletal structure, resulting in different cell deformability ^{131,132}. For example, Pajerowski *et al.* studied that nuclei of human embryonic stem cells become six times stiffer after being terminally differentiated ¹³³.

Similarly, Chowdhury *et al.* found that differentiated mouse embryonic stem cells have 10-fold stiffer than their undifferentiated stage ¹³⁴. Although it has been realized that biological and mechanical factors are correlated to each other during differentiation, what molecule changes result in such differences has not been fully unveiled yet. Measuring the mechanical properties of stem cells at each differentiation stage will provide clues to answer this question.

The separation/enrichment based on stem cell mechanical properties, as a label-free biomarker, has a tremendous potential usage for regenerative medicine. Ekpenyong *et al.* observed that cell viscoelastic properties change determines the fate and function of the myeloid precursor cells in the blood and suggested it as a cell differentiation marker that could use for therapeutic purposes ¹³⁵. Gonzalez-Cruz *et al.* also mentioned that sorting-based enrichment using mechanical biomarkers (*i.e.*, elastic and viscoelastic properties) of adipose-derived stem cells, correlating with the ability to produce tissue-specific metabolites, enables implications for cell-based regenerative therapies ¹³⁶. As another evidence, Bongiorno *et al.* reported that cell stiffness as a single-cell osteoblast differentiation biomarker allows enhanced enrichment of starting cell populations for the stem cell therapies ¹³⁷. Those words may well suggest that the mechanical properties of stem cells are an excellent enrichment target for regenerative medicine therapies.

The pluripotent stem cells have the potential to differentiate into any type of cell in the body. Therefore, implantation of differentiated cells from pluripotent stem cells is a promising approach to cure diseases such as heart failure, retinal and macular degenerations, tendon ruptures, diabetes type 1, immune-system disorders, and neurological diseases. However, many risk factors require special attention for wide-range of stem cell implementation (*e.g.*, stem inaccurate cells types, the variation of differentiation status, proliferation capacity, contamination during in vitro culture and other manipulation steps, irreversibility of treatment, high risk of tumor formation, unwanted immune responses and the transmission of adventitious agents) ^{138,139}. According to the Food Drug Administration (FDA), quality-control is essential in manufacturing cellular therapy products to reduce such risks in stem cell-based therapies ¹⁴⁰. The high-throughput microfluidic devices, which separate cells based on their mechanical phenotypes, can play an essential role in quality control for stem cell-based therapies by providing the scalable cell separation tool to eliminate the tumor-forming stem cells ¹³³ and to collect the mesenchymal stem cells [139] selectively.

5.3 Cancer Cells

It has been realized that cell mechanical phenotyping is a sensitive biomarker to identify cancer cell malignancy ¹⁴¹. Thus, high-throughput mechanotyping approaches have always been of great interest in cytopathology research, where sensitive, quantitative, and automated cytological analysis are often required. The nuclear architecture of cytoplasm (*e.g.*, chromatin condensation, nuclear envelope shape, metaphase nuclei, and the nuclear-cytoplasmic ratio) targets the conventional diagnosis of potential malignancy of cancer cells ^{142,143}. However, unreliable sensitivity (40-90%) of such technique often missed the malignant samples, leading to inappropriate clinical decision and treatment ¹⁴⁴. Besides, long processing time and expensive assay costs due to the complex manual sample preparation (*e.g.*, staining for labeling) and prescreening are often burdens for patients in a clinical setting.

Unlike the conventional approach, mechanical phenotyping facilitates label-free assay for rapid identification of cancer malignancy with minimal hands-on work and short processing time. Besides, high-throughput quantitative analyses can provide standardized metrics for risk assessment of malignancy, which is quite challenging to be achieved by qualitative analysis such as high-resolution imaging ¹⁴⁵. Currently, mechanotyping-based approaches have been extensively applied to translational cancer researches. For example, Yu et al.'s recent work reported that urothelial cell becomes more deformable during malignant transformation and progression mainly because of epithelial-mesenchymal transition pathway ¹⁴⁶. Tse *et al.* showed a quantitative diagnosis of malignant pleural effusions and the ability to distinguish leukemias from inflammatory processes using label-free biophysical markers ¹⁴⁷. Similarly, Remmerbach *et al.* facilitated the screening of suspicious lesions in the oral cavity using quantitative biophysical markers for oral cancer diagnosis ¹⁴⁸. Such examples suggest the significant impact of mechanotyping-based technologies on the clinical decision-making of various cancers.

5.4 Drug Testing

Drug for cancers or diseases affects cytoskeletal or nuclear properties, such as estramustine, discodermolide, and chloroquine ¹⁴⁹⁻¹⁵¹. They influence cell mechanics by modifying the cytoskeletal function, like adjusting the microtubule dynamics or increase oxidative stress ^{150,151}. These cell mechanical property changes will provide a potential biomarker for drug efficacy evaluation and drug screening. More specifically, drug efficacy can be quickly evaluated by changes in the mechanical property of cells before and after the drug treatment because mechanical

properties are expected to have a discernible change if the drug is effective. Otherwise, cells have almost no change due to drug resistance.

It has been long recognized that each disease shows a difference in clinical response to the drug from person to person in clinical treatment. Compared with the traditional bulk-lysed drug screening method, measuring single-cell mechanical properties better represents drug response and tolerance in a heterogeneous population. Besides, the traditional screening method is based on the observation of cell death rate, and it involves hundreds of thousands, or even millions of tests to find the effective drug compounds. Such time demanding process is particularly problematic to develop new drugs quickly for the emergence and spread of drug-resistant pathogens (e.g., malaria) ¹⁵². The availability of the microfluidic mechanotyping device that analyzes thousands of single cells at a second will bring a new approach for high-throughput and quantitative drug screening and drug candidate selection. In the meantime, mechanotype-based cell sorting can be used to enrich the screening libraries for drugs, affecting the architecture of the cytoskeleton or nucleus. Establishing the mechanical property as a standard mode of drug action will provide a positive insight for advanced personalized medicine and drug treatment ¹⁵³.

6 Perspectives and Outlooks

Microfluidics has emerged as a promising technology to retrieve quantitative insight into cell mechanics due to easy manipulation and analysis at the cellular scale. Numerous microfluidic systems implemented the time-dependent characterization of cell deformation and its size, shape, and stress/strain relaxation to understand the relation between the mechanical properties of cells and their function. These tools are now establishing the foundation for mechanical phenotyping research to be translated into clinical applications. Toward the successful translation, the following agenda need to be addressed in the future.

Standardization among various testing approaches. Lack of standardization among various characterization techniques causes analytical challenges and limits the cross-study comparison. Standardized cell deformation technique, detection readout, experimental protocol/setup, and result interpretation guidelines are urgently needed for future microfluidic single-cell mechanotyping device development.

Molecular specificity. The label-free deformability cytometry still lacks molecular specificity,

commonly used to monitor the cellular physiologic states. In standard flow cytometry technology, molecular specificity is achieved by the fluorescent probes ¹⁵⁴. Similarly, the fluorescent readout can be integrated into real-time deformability cytometry for characterizing both the mechanical and physical properties of cells ⁷². Furthermore, hybrid measurement opens the possibility for a correlational study between cell mechanics and molecular properties at the single-cell level.

High-throughput deformability-activated sorting. One direction of future research would be to increase the throughput of deformability-activated cell sorting. As discussed, the real-time deformability analysis enables active sorting based on the mechanical properties of the cell. While automation of continuous-flow individual cell sorting is of high interest to clinicians and cell biologists, the deficiency in sorting speed, compared to the traditional FACS (30,000 – 40,000 cells/s), limits the practical implementation of this technology. Further throughput improvements are expected through parallelization of the system using multiplexed techniques ^{155,156}.

High-throughput single-cell mechanical phenotyping using microfluidics is in the early stage of translation. Label-free deformability analysis provides additional aspects that are unclear in conventional assay due to the high-phenotypic heterogeneity and inconsistent expression of traditional biomarkers ^{157,158}. Moreover, label-free sorting offers enrichment of cells of interest and streamline clinical decision-making. The advancement of microfluidic tools will find various applications such as molecular delivery ^{159,160} and cell-fate decisions ^{130,161}, where label-free single-cell mechanotyping is desired.

7 Acknowledgements

This work is partially supported by the National Institutes of Health (R61AI147419). The content is solely the responsibility of the authors and does not necessarily represent the official views of the National Institutes of Health. W.G. acknowledges support from the Penn State Startup Fund.

Figure captions

Figure 1. Physical constriction microfluidic device with various geometries and readouts for cell deformability measurement. (a) The conductance changes were monitored when the cell squeezed through the constriction pore. The width of the signal peak indicates the transit time ²⁸. (b) Two consecutive constrictions with different widths were used for cell size and deformability measurement ³⁰. Transit time was electrically measured. (c) Size-independent deformability cytometry using real-time adjustable constriction ³¹. The system can control the constriction height for polydisperse samples in size. The cell transit velocity (or time) information was extracted from a time-dependent cell position in the microfluidic channel. (d) Microfluidic constriction-based pressure manometer ³². The y-positional change directly indicated the pressure drop across the constriction during the cell translocation event.

Figure 2. Various multi-constriction methods. (a) Deformability-based flow cytometry using series constrictions ³⁵. (b) Microfluidic cell-phoresis device using sequential constriction in parallel ³⁷. (c) Quantitative deformability cytometry using parallel constriction array for rapid and calibrated measurement ³⁸. (d) Parallelized differential multi-constrictions in series for cell deformation and relaxation measurement ⁴⁰.

Figure 3. Cell deformation using various hydrodynamic stretching microfluidic device geometry: (a) Cross-junction ⁴¹, (b) hydro-pipetting with cross-junction ⁴², (c) funnel shape ⁴³, (d) funnel-shaped fluidic channel array ⁴⁴.

Figure 4. Schematics of various deformability measurement methods. (a) deformability was measured by the aspect ratio changes of the cell using image processing. (b) cell position and time are extracted by image analysis, yielding the transit time (indirect deformability indicator) of cell translocation at a funnel-shaped constriction channel. (c) DC sensing was used to obtain the ionic current dips, providing cell transit time. (d) The AC measurement monitored resistance/impedance change to obtain the transit time. (e) Mechanical cantilever measures the buoyant forces and their resonant frequency. The transit time, entry time, and passage time can be extracted from the resonant frequency profile.

Figure 5. Various label-free, continuous, and passive bulk cell separation based on cell deformability: (a) porous membrane microfiltration using crossflow ⁷⁵. While larger and stiffer white blood cells are captured at the filter entrance, small and softer red blood cells pass through the filter. (b) deterministic lateral displacement ⁹⁰. Repeated laminar flow fields were depicted with a circular post array. Stiffer cells shift the streamlines as they pass through the post array while soft cells are deformed and remained in the original streamline. (c) diagonal compression ridge ⁹⁵. Soft cells are displaced in a negative transverse direction from the channel axis, while ridge cells while stiff ones are moving in the positive transverse direction. Two sheath flows aligned the cells at the channel axis. (d) resettable cell traps ¹⁰². The constricted diaphragm forms the traps to capture the cells of interest, while unwanted cells flow through the traps and collected in the waste outlet. Relaxed diaphragm enlarged the channel dimension to clear the microchannel. (e) microfluidic ratchet-sorter ¹⁰⁶. Continuous deformability-based cell separation using oscillatory flow and tapered contractions. The more deformable cells travel further up than stiffer ones. Crossflow propels the cells in the horizontal direction toward the collection outlets. (f) inertial microfluidics

¹¹⁰. Inertial lift force (F_L) and viscoelasticity induced force (F_V) are counter-interacted, determining the effective cell position in the channel. The deformable cells tend to stay in the center of the channel axis, while stiff cells move toward the channel walls.

Figure 6. Various active sorting approaches for a single cell or particle. (a) Optical stretcher integrated with optofluidic sorter ¹¹². Blue channels depict the fluidic channels. Red channels indicate the optical channels. Index matching fluid was filled in the red optical channels. (b) soRT-FDC ⁷⁰. RT-FDC was integrated with a downstream standing surface acoustic wave (SSAW)-based active cell sorter. Three-channel fluorescence imaging was integrated for specificity. (c) Deformability-activated microfluidic particle sorting device ⁷¹. Constriction-based deformability sensor real-time extracts the cell transit time, which was used as a sorting trigger. After deformability measurement, the hydrodynamic sorting mechanism deflects the particle toward the designated collection outlet.

References

- 1 El-Ali, J., Sorger, P. K. & Jensen, K. F. Cells on chips. *Nature* 2006;**442**:403-411.
- 2 Fritsch, A., Hockel, M., Kiessling, T., Nnetu, K. D., Wetzel, F., Zink, M. & Kas, J. A. Are biomechanical changes necessary for tumour progression? *Nat Phys* 2010;**6**:730-732.
- Moraes, C., Sun, Y. & Simmons, C. A. (Micro)managing the mechanical microenvironment. *Integr Biol-Uk* 2011;**3**:959-971.
- 4 Li, J., Lykotrafitis, G., Dao, M. & Suresh, S. Cytoskeletal dynamics of human erythrocyte. *P Natl Acad Sci USA* 2007;**104**:4937-4942.
- 5 Swift, J. & Discher, D. E. The nuclear lamina is mechano-responsive to ECM elasticity in mature tissue. *J Cell Sci* 2014;**127**:3005-3015.
- 6 Isermann, P. & Lammerding, J. Nuclear mechanics and mechanotransduction in health and disease. *Curr Biol* 2013;**23**:R1113-1121.
- Yang, X. N., Chen, Z. F., Miao, J., Cui, L. W. & Guan, W. H. High-throughput and label-free parasitemia quantification and stage differentiation for malaria-infected red blood cells. *Biosensors & bioelectronics* 2017;**98**:408-414.
- 8 Alapan, Y., Little, J. A. & Gurkan, U. A. Heterogeneous red blood cell adhesion and deformability in sickle cell disease. *Scientific reports* 2014;**4**:7173.
- 9 Nishino, M., Tanaka, H., Ogura, H., Inoue, Y., Koh, T., Fujita, K. & Sugimoto, H. Serial changes in leukocyte deformability and whole blood rheology in patients with sepsis or trauma. *The Journal of trauma* 2005;**59**:1425-1431.
- 10 Byun, S., Son, S., Amodei, D., Cermak, N., Shaw, J., Kang, J. H., Hecht, V. C., Winslow, M. M., Jacks, T., Mallick, P. & Manalis, S. R. Characterizing deformability and surface friction of cancer cells. *Proc Natl Acad Sci U S A* 2013;110:7580-7585.
- 11 Di Carlo, D. A mechanical biomarker of cell state in medicine. *J Lab Autom* 2012;**17**:32-42.
- 12 Guzniczak, E., Mohammad Zadeh, M., Dempsey, F., Jimenez, M., Bock, H., Whyte, G., Willoughby, N. & Bridle, H. High-throughput assessment of mechanical properties of stem cell derived red blood cells, toward cellular downstream processing. *Scientific reports* 2017;7:14457.
- 13 Wen, J. H., Vincent, L. G., Fuhrmann, A., Choi, Y. S., Hribar, K. C., Taylor-Weiner, H., Chen, S. & Engler, A. J. Interplay of matrix stiffness and protein tethering in stem cell differentiation. *Nature materials* 2014;**13**:979-987.
- 14 Bongiorno, T., Kazlow, J., Mezencev, R., Griffiths, S., Olivares-Navarrete, R., McDonald, J. F., Schwartz, Z., Boyan, B. D., McDevitt, T. C. & Sulchek, T. Mechanical stiffness as

- an improved single-cell indicator of osteoblastic human mesenchymal stem cell differentiation. *Journal of biomechanics* 2014;**47**:2197-2204.
- 15 Jin, H., Xing, X., Zhao, H., Chen, Y., Huang, X., Ma, S., Ye, H. & Cai, J. Detection of erythrocytes influenced by aging and type 2 diabetes using atomic force microscope. *Biochemical and biophysical research communications* 2010;**391**:1698-1702.
- 16 Lekka, M., Laidler, P., Gil, D., Lekki, J., Stachura, Z. & Hrynkiewicz, A. Elasticity of normal and cancerous human bladder cells studied by scanning force microscopy. *European Biophysics Journal* 1999;**28**:312-316.
- 17 Hochmuth, R. M. Micropipette aspiration of living cells. *J Biomech* 2000;**33**:15-22.
- 18 Rand, R. P. Mechanical Properties of the Red Cell Membrane. Ii. Viscoelastic Breakdown of the Membrane. *Biophys. J.* 1964;4:303-316.
- 19 Guck, J., Ananthakrishnan, R., Moon, T. J., Cunningham, C. C. & Kas, J. Optical deformability of soft biological dielectrics. *Phys Rev Lett* 2000;**84**:5451-5454.
- 20 Jonietz, E. MECHANICS The forces of cancer. *Nature* 2012;491:S56-S57.
- 21 Lincoln, B., Erickson, H. M., Schinkinger, S., Wottawah, F., Mitchell, D., Ulvick, S., Bilby, C. & Guck, J. Deformability-based flow cytometry. *Cytom Part A* 2004;**59a**:203-209.
- 22 Guck, J., Schinkinger, S., Lincoln, B., Wottawah, F., Ebert, S., Romeyke, M., Lenz, D., Erickson, H. M., Ananthakrishnan, R., Mitchell, D., Kas, J., Ulvick, S. & Bilby, C. Optical deformability as an inherent cell marker for testing malignant transformation and metastatic competence. *Biophys. J.* 2005;88:3689-3698.
- 23 Hwang, J. Y., Kim, J., Park, J. M., Lee, C., Jung, H., Lee, J. & Shung, K. K. Cell Deformation by Single-beam Acoustic Trapping: A Promising Tool for Measurements of Cell Mechanics. *Scientific reports* 2016;6:27238.
- 24 Wang, H., Liu, Z., Shin, D. M., Chen, Z. G., Cho, Y., Kim, Y. J. & Han, A. A continuous-flow acoustofluidic cytometer for single-cell mechanotyping. *Lab Chip* 2019;**19**:387-393.
- 25 Gueguen, R. M., Bidet, J. M., Durand, F., Driss, F., Joffre, A. & Genetet, B. Filtration Pressure and Red-Blood-Cell Deformability 1st Results Obtained with a New Device Erythrometer. *Biorheology* 1983;**20**:830-830.
- 26 Nakamura, T., Hasegawa, S., Shio, H. & Uyesaka, N. Rheologic and Pathophysiologic Significance of Red-Cell Passage through Narrow Pores. *Blood* 1993;**82**:A3-A3.
- 27 Lange, J. R., Steinwachs, J., Kolb, T., Lautscham, L. A., Harder, I., Whyte, G. & Fabry, B. Microconstriction Arrays for High-Throughput Quantitative Measurements of Cell Mechanical Properties. *Biophys. J.* 2015;**109**:26-34.

- 28 Zheng, Y., Shojaei-Baghini, E., Azad, A., Wang, C. & Sun, Y. High-throughput biophysical measurement of human red blood cells. *Lab on a Chip* 2012;**12**:2560-2567.
- 29 Zheng, Y., Nguyen, J., Wang, C. & Sun, Y. Electrical measurement of red blood cell deformability on a microfluidic device. *Lab on a Chip* 2013;**13**:3275-3283.
- 30 Sano, M., Kaji, N., Rowat, A. C., Yasaki, H., Shao, L., Odaka, H., Yasui, T., Higashiyama, T. & Baba, Y. Microfluidic Mechanotyping of a Single Cell with Two Consecutive Constrictions of Different Sizes and an Electrical Detection System. *Anal Chem* 2019;91(20):12890–12899.
- 31 Guan, G. F., Chen, P. C. Y., Peng, W. K., Bhagat, A. A., Ong, C. J. & Han, J. Y. Real-time control of a microfluidic channel for size-independent deformability cytometry. *J Micromech Microeng* 2012;**22**:105037-105044.
- 32 Abkarian, M., Faivre, M. & Stone, H. A. High-speed microfluidic differential manometer for cellular-scale hydrodynamics. *P Natl Acad Sci USA* 2006;**103**:538-542.
- 33 Kollmannsberger, P. & Fabry, B. Linear and Nonlinear Rheology of Living Cells. *Annu Rev Mater Res* 2011;**41**:75-97.
- 34 Nyberg, K. D., Scott, M. B., Bruce, S. L., Gopinath, A. B., Bikos, D., Mason, T. G., Kim, J. W., Choi, H. S. & Rowat, A. C. The physical origins of transit time measurements for rapid, single cell mechanotyping. *Lab on a Chip* 2016;**16**:3330 3339.
- 35 Bow, H., Pivkin, I. V., Diez-Silva, M., Goldfless, S. J., Dao, M., Niles, J. C., Suresh, S. & Han, J. Y. A microfabricated deformability-based flow cytometer with application to malaria. *Lab on a Chip* 2011;**11**:1065-1073.
- 36 Rowat, A. C., Jaalouk, D. E., Zwerger, M., Ung, W. L., Eydelnant, I. A., Olins, D. E., Olins, A. L., Herrmann, H., Weitz, D. A. & Lammerding, J. Nuclear Envelope Composition Determines the Ability of Neutrophil-type Cells to Passage through Micron-scale Constrictions. *J Biol Chem* 2013;**288**:8610-8618.
- 37 Santoso, A. T., Deng, X., Lee, J.-H., Matthews, K., Duffy, S. P., Islamzada, E., McFaul, S. M., Myrand-Lapierre, M.-E. & Ma, H. Microfluidic cell-phoresis enabling high-throughput analysis of red blood cell deformability and biophysical screening of antimalarial drugs. *Lab on a Chip* 2015;**15**:4451-4460.
- 38 Nyberg, K. D., Hu, K. H., Kleinman, S. H., Khismatullin, D. B., Butte, M. J. & Rowat, A. C. Quantitative Deformability Cytometry: Rapid, Calibrated Measurements of Cell Mechanical Properties. *Biophys. J.* 2017;**113**:1574-1584.
- 39 Rosenbluth, M. J., Lam, W. A. & Fletcher, D. A. Analyzing cell mechanics in hematologic diseases with microfluidic biophysical flow cytometry. *Lab on a Chip* 2008;**8**:1062-1070.
- 40 Yang, D., Zhou, Y., Zhou, Y., Han, J. & Ai, Y. Biophysical phenotyping of single cells using a differential multiconstriction microfluidic device with self-aligned 3D electrodes.

- *Biosensors and Bioelectronics* 2019;**133**:16-23.
- 41 Gossett, D. R., Tse, H. T. K., Lee, S. A., Ying, Y., Lindgren, A. G., Yang, O. O., Rao, J. Y., Clark, A. T. & Di Carlo, D. Hydrodynamic stretching of single cells for large population mechanical phenotyping. *P Natl Acad Sci USA* 2012;**109**:7630-7635.
- 42 Dudani, J. S., Gossett, D. R., Tse, H. T. K. & Di Carlo, D. Pinched-flow hydrodynamic stretching of single-cells. *Lab on a Chip* 2013;**13**:3728-3734.
- 43 Otto, O., Rosendahl, P., Mietke, A., Golfier, S., Herold, C., Klaue, D., Girardo, S., Pagliara, S., Ekpenyong, A., Jacobi, A., Wobus, M., Topfner, N., Keyser, U. F., Mansfeld, J., Fischer-Friedrich, E. & Guck, J. Real-time deformability cytometry: on-the-fly cell mechanical phenotyping. *Nat Methods* 2015;12:199-202.
- 44 Ahmmed, S. M., Bithi, S. S., Pore, A. A., Mubtasim, N., Schuster, C., Gollahon, L. S. & Vanapalli, S. A. Multi-sample deformability cytometry of cancer cells. *Apl Bioeng* 2018;**2**:032002.
- 45 Di Carlo, D., Irimia, D., Tompkins, R. G. & Toner, M. Continuous inertial focusing, ordering, and separation of particles in microchannels. *P Natl Acad Sci USA* 2007;**104**:18892-18897.
- 46 Cha, S., Shin, T., Lee, S. S., Shim, W., Lee, G., Lee, S. J., Kim, Y. & Kim, J. M. Cell Stretching Measurement Utilizing Viscoelastic Particle Focusing. *Analytical Chemistry* 2012;84:10471-10477.
- 47 Armistead, F. J., De Pablo, J. G., Gadêlha, H., Peyman, S. A. & Evans, S. D. Cells under stress: an inertial-shear microfluidic determination of cell behavior. *Biophys. J.* 2019;**116**:1127-1135.
- 48 Sawetzki, T., Eggleton, C. D., Desai, S. A. & Marr, D. W. M. Viscoelasticity as a Biomarker for High-Throughput Flow Cytometry. *Biophys. J.* 2013;**105**:2281-2288.
- 49 Darling, E. M., Zauscher, S. & Guilak, F. Viscoelastic properties of zonal articular chondrocytes measured by atomic force microscopy. *Osteoarthritis Cartilage* 2006;**14**:571-579.
- 50 Mierke, C. T. The role of the optical stretcher is crucial in the investigation of cell mechanics regulating cell adhesion and motility. *Frontiers in cell and developmental biology* 2019;7:184.
- 51 Wu, H. W., Kuhn, T. & Moy, V. T. Mechanical properties of 1929 cells measured by atomic force microscopy: Effects of anticytoskeletal drugs and membrane crosslinking. *Scanning* 1998;**20**:389-397.
- 52 Roth, K. B., Neeves, K. B., Squier, J. & Marr, D. W. High throughput linear optical stretcher for mechanical characterization of blood cells. *Cytom Part A* 2016;**89**:391-397.

- 53 Tsukada, K., Sekizuka, E., Oshio, C. & Minamitani, H. Direct measurement of erythrocyte deformability in diabetes mellitus with a transparent microchannel capillary model and high-speed video camera system. *Microvasc Res* 2001;**61**:231-239.
- 54 Forsyth, A. M., Wan, J., Ristenpart, W. D. & Stone, H. A. The dynamic behavior of chemically "stiffened" red blood cells in microchannel flows. *Microvasc Res* 2010;**80**:37-43.
- 55 Lee, S. S., Yim, Y., Ahn, K. H. & Lee, S. J. Extensional flow-based assessment of red blood cell deformability using hyperbolic converging microchannel. *Biomed Microdevices* 2009;**11**:1021-1027.
- 56 Forsyth, A. M., Wan, J. D., Owrutsky, P. D., Abkarian, M. & Stone, H. A. Multiscale approach to link red blood cell dynamics, shear viscosity, and ATP release. *P Natl Acad Sci USA* 2011;**108**:10986-10991.
- 57 Tomaiuolo, G., Barra, M., Preziosi, V., Cassinese, A., Rotoli, B. & Guido, S. Microfluidics analysis of red blood cell membrane viscoelasticity. *Lab on a Chip* 2011;**11**:449-454.
- 58 Hou, H. W., Li, Q. S., Lee, G. Y. H., Kumar, A. P., Ong, C. N. & Lim, C. T. Deformability study of breast cancer cells using microfluidics. *Biomed Microdevices* 2009;**11**:557-564.
- 59 Shelby, J. P., White, J., Ganesan, K., Rathod, P. K. & Chiu, D. T. A microfluidic model for single-cell capillary obstruction by Plasmodium falciparum infected erythrocytes. *P Natl Acad Sci USA* 2003;**100**:14618-14622.
- 60 Katsumoto, Y., Tatsumi, K., Doi, T. & Nakabe, K. Electrical classification of single red blood cell deformability in high-shear microchannel flows. *Int J Heat Fluid Fl* 2010;**31**:985-995.
- 61 Adamo, A., Sharei, A., Adamo, L., Lee, B., Mao, S. & Jensen, K. F. Microfluidics-Based Assessment of Cell Deformability. *Analytical Chemistry* 2012;**84**:6438-6443.
- 62 Burg, T. P. & Manalis, S. R. Suspended microchannel resonators for biomolecular detection. *Appl Phys Lett* 2003;**83**:2698-2700.
- 63 Burg, T. P. & Manalis, S. R. Microfluidic packaging of suspended microchannel resonators for biomolecular detection. *Eng Med Biol Soc Ann* 2005;264-267.
- 64 Grover, W. H., Bryan, A. K., Diez-Silva, M., Suresh, S., Higgins, J. M. & Manalis, S. R. Measuring single-cell density. *P Natl Acad Sci USA* 2011;**108**:10992-10996.
- 65 Godin, M., Bryan, A. K., Burg, T. P., Babcock, K. & Manalis, S. R. Measuring the mass, density, and size of particles and cells using a suspended microchannel resonator. *Appl Phys Lett* 2007;**91**:123121.
- 66 Bryan, A. K., Hecht, V. C., Shen, W. J., Payer, K., Grover, W. H. & Manalis, S. R. Measuring single cell mass, volume, and density with dual suspended microchannel

- resonators. Lab on a Chip 2014;14:569-576.
- 67 Urbanska, M., Munoz, H. E., Shaw Bagnall, J., Otto, O., Manalis, S. R., Di Carlo, D. & Guck, J. A comparison of microfluidic methods for high-throughput cell deformability measurements. *Nat Methods* 2020.
- 68 Deng, Y. X., Davis, S. P., Yang, F., Paulsen, K. S., Kumar, M., DeVaux, R. S., Wang, X. H., Conklin, D. S., Oberai, A., Herschkowitz, J. I. & Chung, A. J. Inertial Microfluidic Cell Stretcher (iMCS): Fully Automated, High-Throughput, and Near Real-Time Cell Mechanotyping. *Small* 2017;13:1700705.
- 69 Zhou, Y., Yang, D. H., Zhou, Y. N., Khoo, B. L., Han, J. & Ai, Y. Characterizing Deformability and Electrical Impedance of Cancer Cells in a Microfluidic Device. *Analytical Chemistry* 2018;**90**:912-919.
- 70 Nawaz, A. A., Urbanska, M., Herbig, M., Notzel, M., Krater, M., Rosendahl, P., Herold, C., Toepfner, N., Kubankova, M., Goswami, R., Abuhattum, S., Reichel, F., Muller, P., Taubenberger, A., Girardo, S., Jacobi, A. & Guck, J. Intelligent image-based deformation-assisted cell sorting with molecular specificity. *Nat Methods* 2020;17:595-599.
- 71 Choi, G., Nouri, R., Zarzar, L. & Guan, W. Microfluidic deformability-activated sorting of single particles. *Microsystems & Nanoengineering* 2020;**6**:1-9.
- 72 Rosendahl, P., Plak, K., Jacobi, A., Kraeter, M., Toepfner, N., Otto, O., Herold, C., Winzi, M., Herbig, M., Ge, Y., Girardo, S., Wagner, K., Baum, B. & Guck, J. Real-time fluorescence and deformability cytometry. *Nat Methods* 2018;**15**:355-358.
- 73 Di Carlo, D. & Lee, L. P. Dynamic single-cell analysis for quantitative biology. *Analytical Chemistry* 2006;**78**:7918-7925.
- 74 Lee, W., Tseng, P. & Carlo, D. D. *Microtechnology for cell manipulation and sorting*. 1-14 (Springer Berlin Heidelberg, 2017).
- 75 Li, X., Chen, W. Q., Liu, G. Y., Lu, W. & Fu, J. P. Continuous-flow microfluidic blood cell sorting for unprocessed whole blood using surfacemicromachined microfiltration membranes. *Lab on a Chip* 2014;**14**:2565-2575.
- 76 Cheng, Y. N., Ye, X. Y., Ma, Z. S., Xie, S. & Wang, W. H. High-throughput and clogging-free microfluidic filtration platform for on-chip cell separation from undiluted whole blood. *Biomicrofluidics* 2016;**10**:014118.
- 77 Kang, Y. T., Doh, I., Byun, J., Chang, H. J. & Cho, Y. H. Label-free Rapid Viable Enrichment of Circulating Tumor Cell by Photosensitive Polymer-based Microfilter Device. *Theranostics* 2017;7:3179-3191.
- 78 Ji, H. M., Samper, V., Chen, Y., Heng, C. K., Lim, T. M. & Yobas, L. Silicon-based microfilters for whole blood cell separation. *Biomed Microdevices* 2008;**10**:251-257.

- 79 Zhang, W. J., Kai, K., Choi, D. S., Iwamoto, T., Nguyen, Y. H., Wong, H. L., Landis, M. D., Ueno, N. T., Chang, J. & Qin, L. D. Microfluidics separation reveals the stem-cell-like deformability of tumor-initiating cells. *P Natl Acad Sci USA* 2012;**109**:18707-18712.
- 80 Alvankarian, J., Bahadorimehr, A. & Majlis, B. Y. A pillar-based microfilter for isolation of white blood cells on elastomeric substrate. *Biomicrofluidics* 2013;7:014102.
- 81 Wu, C. C., Hong, L. Z. & Ou, C. T. Blood Cell-free Plasma Separated from Blood Samples with a Cascading Weir-type Microfilter Using Dead-end Filtration. *J Med Biol Eng* 2012;**32**:163-168.
- 82 Crowley, T. A. & Pizziconi, V. Isolation of plasma from whole blood using planar microfilters for lab-on-a-chip applications. *Lab on a Chip* 2005;**5**:922-929.
- 83 Gill, N. K., Ly, C., Nyberg, K. D., Lee, L., Qi, D., Tofig, B., Reis-Sobreiro, M., Dorigo, O., Rao, J., Wiedemeyer, R., Karlan, B., Lawrenson, K., Freeman, M. R., Damoiseaux, R. & Rowat, A. C. A scalable filtration method for high throughput screening based on cell deformability. *Lab Chip* 2019;**19**:343-357.
- 84 Sethu, P., Sin, A. & Toner, M. Microfluidic diffusive filter for apheresis (leukapheresis). *Lab on a Chip* 2006;**6**:83-89.
- 85 Dalili, A., Samiei, E. & Hoorfar, M. A review of sorting, separation and isolation of cells and microbeads for biomedical applications: microfluidic approaches. *Analyst* 2019;**144**:87-113.
- 86 Huang, L. R., Cox, E. C., Austin, R. H. & Sturm, J. C. Continuous particle separation through deterministic lateral displacement. *Science* 2004;**304**:987-990.
- 87 McGrath, J., Jimenez, M. & Bridle, H. Deterministic lateral displacement for particle separation: a review. *Lab on a Chip* 2014;**14**:4139-4158.
- 88 Beech, J. P., Holm, S. H., Adolfsson, K. & Tegenfeldt, J. O. Sorting cells by size, shape and deformability. *Lab on a Chip* 2012;**12**:1048-1051.
- 89 Kruger, T., Holmes, D. & Coveney, P. V. Deformability-based red blood cell separation in deterministic lateral displacement devices-A simulation study. *Biomicrofluidics* 2014;8:054114.
- 90 Xavier, M., Holm, S. H., Beech, J. P., Spencer, D., Tegenfeldt, J. O., Oreffo, R. O. C. & Morgan, H. Label-free enrichment of primary human skeletal progenitor cells using deterministic lateral displacement. *Lab on a Chip* 2019;**19**:513-523.
- 91 Holmes, D., Whyte, G., Bailey, J., Vergara-Irigaray, N., Ekpenyong, A., Guck, J. & Duke, T. Separation of blood cells with differing deformability using deterministic lateral displacement. *Interface Focus* 2014;4:20140011.
- 92 Al-Fandi, M., Al-Rousan, M., Jaradat, M. A. K. & Al-Ebbini, L. New design for the

- separation of microorganisms using microfluidic deterministic lateral displacement. *Robot Cim-Int Manuf* 2011;**27**:237-244.
- 93 Zhang, Z. M., Henry, E., Gompper, G. & Fedosov, D. A. Behavior of rigid and deformable particles in deterministic lateral displacement devices with different post shapes. *J Chem Phys* 2015;**143**:243145.
- 94 Zhang, Z. M., Chien, W., Henry, E., Fedosov, D. A. & Gompper, G. Sharp-edged geometric obstacles in microfluidics promote deformability-based sorting of cells. *Phys Rev Fluids* 2019;4:024201.
- 95 Islam, M., Brink, H., Blanche, S., DiPrete, C., Bongiorno, T., Stone, N., Liu, A., Philip, A., Wang, G. H., Lam, W., Alexeev, A., Waller, E. K. & Sulchek, T. Microfluidic Sorting of Cells by Viability Based on Differences in Cell Stiffness. *Scientific reports* 2017;7:1-12.
- 96 Wang, G. H., Mao, W. B., Byler, R., Patel, K., Henegar, C., Alexeev, A. & Sulchek, T. Stiffness Dependent Separation of Cells in a Microfluidic Device. *Plos One* 2013;8:e75901.
- 97 Arata, J. P. & Alexeev, A. Designing microfluidic channel that separates elastic particles upon stiffness. *Soft Matter* 2009;**5**:2721-2724.
- 98 Wang, G. H., Crawford, K., Turbyfield, C., Lam, W., Alexeev, A. & Sulchek, T. Microfluidic cellular enrichment and separation through differences in viscoelastic deformation. *Lab on a Chip* 2015;**15**:532-540.
- 99 Chang, Y. H., Huang, C. J. & Lee, G. B. A tunable microfluidic-based filter modulated by pneumatic pressure for separation of blood cells. *Microfluid Nanofluid* 2012;**12**:85-94.
- 100 Huang, S. B., Wu, M. H. & Lee, G. B. A tunable micro filter modulated by pneumatic pressure for cell separation. *Sensor Actuat B-Chem* 2009;**142**:389-399.
- 101 Beattie, W., Qin, X., Wang, L. & Ma, H. S. Clog-free cell filtration using resettable cell traps. *Lab on a Chip* 2014;**14**:2657-2665.
- 102 Qin, X., Park, S., Duffy, S. P., Matthews, K., Ang, R. R., Todenhofer, T., Abdi, H., Azad, A., Bazov, J., Chi, K. N., Black, P. C. & Ma, H. S. Size and deformability based separation of circulating tumor cells from castrate resistant prostate cancer patients using resettable cell traps. *Lab on a Chip* 2015;**15**:2278-2286.
- 103 Guo, Q., McFaul, S. M. & Ma, H. S. Deterministic microfluidic ratchet based on the deformation of individual cells. *Phys Rev E* 2011;**83**:051910.
- 104 McFaul, S. M., Lin, B. K. & Ma, H. S. Cell separation based on size and deformability using microfluidic funnel ratchets. *Lab on a Chip* 2012;**12**:2369-2376.
- 105 Guo, Q., Duffy, S. P., Matthews, K., Islamzada, E. & Ma, H. S. Deformability based Cell

- Sorting using Microfluidic Ratchets Enabling Phenotypic Separation of Leukocytes Directly from Whole Blood. *Scientific reports* 2017;7:1-11.
- 106 Guo, Q., Duffy, S. P., Matthews, K., Deng, X. Y., Santoso, A. T., Islamzada, E. & Ma, H. S. Deformability based sorting of red blood cells improves diagnostic sensitivity for malaria caused by Plasmodium falciparum. *Lab on a Chip* 2016;**16**:645-654.
- 107 Park, E. S., Jin, C., Guo, Q., Ang, R. R., Duffy, S. P., Matthews, K., Azad, A., Abdi, H., Todenhofer, T., Bazov, J., Chi, K. N., Black, P. C. & Ma, H. S. Continuous Flow Deformability-Based Separation of Circulating Tumor Cells Using Microfluidic Ratchets. *Small* 2016;**12**:1909-1919.
- 108 Islamzada, E., Matthews, K., Guo, Q., Santoso, A. T., Duffy, S. P., Scott, M. D. & Ma, H. Deformability based sorting of stored red blood cells reveals donor-dependent aging curves. *Lab Chip* 2020;**20**:226-235.
- 109 Di Carlo, D., Edd, J. F., Irimia, D., Tompkins, R. G. & Toner, M. Equilibrium separation and filtration of particles using differential inertial focusing. *Analytical Chemistry* 2008;**80**:2204-2211.
- 110 Hur, S. C., Henderson-MacLennan, N. K., McCabe, E. R. B. & Di Carlo, D. Deformability-based cell classification and enrichment using inertial microfluidics. *Lab on a Chip* 2011;**11**:912-920.
- 111 Guzniczak, E., Otto, O., Whyte, G., Willoughby, N., Jimenez, M. & Bridle, H. Correction: Deformability-induced lift force in spiral microchannels for cell separation. *Lab Chip* 2020;**20**:1877.
- 112 Faigle, C., Lautenschlager, F., Whyte, G., Homewood, P., Martin-Badosa, E. & Guck, J. A monolithic glass chip for active single-cell sorting based on mechanical phenotyping. *Lab on a Chip* 2015;**15**:1267-1275.
- 113 Nawaz, A. A., Chen, Y., Nama, N., Nissly, R. H., Ren, L., Ozcelik, A., Wang, L., McCoy, J. P., Levine, S. J. & Huang, T. J. Acoustofluidic Fluorescence Activated Cell Sorter. *Anal Chem* 2015;87:12051-12058.
- 114 Li, P. & Ai, Y. Label-Free Multivariate Biophysical Phenotyping-Activated Acoustic Sorting at the Single-Cell Level. *Analytical Chemistry* 2021;**93**:4108-4117.
- 115 Mattanovich, D. & Borth, N. Applications of cell sorting in biotechnology. *Microb Cell Fact* 2006;**5**:1-11.
- 116 Brown, M. & Wittwer, C. Flow cytometry: Principles and clinical applications in hematology. *Clin Chem* 2000;**46**:1221-1229.
- 117 Islam, M., Mezencev, R., McFarland, B., Brink, H., Campbell, B., Tasadduq, B., Waller, E. K., Lam, W., Alexeev, A. & Sulchek, T. Microfluidic cell sorting by stiffness to examine heterogenic responses of cancer cells to chemotherapy. *Cell Death Dis* 2018;**9**:1-12.

- 118 Waugh, R. & Evans, E. A. Thermoelasticity of red blood cell membrane. *Biophys J* 1979;**26**:115-131.
- 119 Tomaiuolo, G. Biomechanical properties of red blood cells in health and disease towards microfluidics. *Biomicrofluidics* 2014;**8**:051501.
- 120 Diez-Silva, M., Dao, M., Han, J. Y., Lim, C. T. & Suresh, S. Shape and Biomechanical Characteristics of Human Red Blood Cells in Health and Disease. *Mrs Bull* 2010;**35**:382-388.
- 121 Mills, J. P., Diez-Silva, M., Quinn, D. J., Dao, M., Lang, M. J., Tan, K. S. W., Lim, C. T., Milon, G., David, P. H., Mercereau-Puijalon, O., Bonnefoy, S. & Suresh, S. Effect of plasmodial RESA protein on deformability of human red blood cells harboring Plasmodium falciparum. *P Natl Acad Sci USA* 2007;**104**:9213-9217.
- 122 Park, Y. K., Diez-Silva, M., Popescu, G., Lykotrafitis, G., Choi, W. S., Feld, M. S. & Suresh, S. Refractive index maps and membrane dynamics of human red blood cells parasitized by Plasmodium falciparum. *P Natl Acad Sci USA* 2008;**105**:13730-13735.
- 123 Cranston, H. A., Boylan, C. W., Carroll, G. L., Sutera, S. P., Williamson, J. R., Gluzman, I. Y. & Krogstad, D. J. Plasmodium-Falciparum Maturation Abolishes Physiologic Red-Cell Deformability. *Science* 1984;223:400-403.
- 124 Zheng, Y., Nguyen, J., Wei, Y. & Sun, Y. Recent advances in microfluidic techniques for single-cell biophysical characterization. *Lab on a Chip* 2013;**13**:2464-2483.
- 125 Kirschenbaum, L. A., Aziz, M., Astiz, M. E., Saha, D. C. & Rackow, E. C. Influence of rheologic changes and platelet-neutrophil interactions on cell filtration in sepsis. *Am J Resp Crit Care* 2000;**161**:1602-1607.
- 126 Kang, J. H., Super, M., Yung, C. W., Cooper, R. M., Domansky, K., Graveline, A. R., Mammoto, T., Berthet, J. B., Tobin, H., Cartwright, M. J., Watters, A. L., Rottman, M., Waterhouse, A., Mammoto, A., Gamini, N., Rodas, M. J., Kole, A., Jiang, A., Valentin, T. M., Diaz, A., Takahashi, K. & Ingber, D. E. An extracorporeal blood-cleansing device for sepsis therapy. *Nat Med* 2014;20:1211-1216.
- 127 Crawford, K., DeWitt, A., Brierre, S., Caffery, T., Jagneaux, T., Thomas, C., Macdonald, M., Tse, H., Shah, A., Di Carlo, D. & O'Neal, H. R. Rapid Biophysical Analysis of Host Immune Cell Variations Associated with Sepsis. *Am J Respir Crit Care Med* 2018;**198**:280-282.
- 128 Wong, S. W., Lenzini, S. & Shin, J. W. Perspective: Biophysical regulation of cancerous and normal blood cell lineages in hematopoietic malignancies. *Apl Bioeng* 2018;**2**:031802.
- 129 Hansen, C. E. & Lam, W. A. Clinical Implications of Single-Cell Microfluidic Devices for Hematological Disorders. *Analytical Chemistry* 2017;**89**:11881-11892.
- 130 Engler, A. J., Sen, S., Sweeney, H. L. & Discher, D. E. Matrix elasticity directs stem cell

- lineage specification. *Cell* 2006;**126**:677-689.
- 131 Nobusue, H., Onishi, N., Shimizu, T., Sugihara, E., Oki, Y., Sumikawa, Y., Chiyoda, T., Akashi, K., Kano, K. & Saya, H. Regulation of MKL1 via actin cytoskeleton dynamics drives adipocyte differentiation. *Mol Biol Cell* 2014;**25**:1-12.
- 132 Labriola, N. R. & Darling, E. M. Temporal heterogeneity in single-cell gene expression and mechanical properties during adipogenic differentiation. *Journal of Biomechanics* 2015;**48**:1058-1066.
- 133 Pajerowski, J. D., Dahl, K. N., Zhong, F. L., Sammak, P. J. & Discher, D. E. Physical plasticity of the nucleus in stem cell differentiation. *P Natl Acad Sci USA* 2007;**104**:15619-15624.
- 134 Chowdhury, F., Li, Y. Z., Poh, Y. C., Yokohama-Tamaki, T., Wang, N. & Tanaka, T. S. Soft Substrates Promote Homogeneous Self-Renewal of Embryonic Stem Cells via Downregulating Cell-Matrix Tractions. *Plos One* 2010;**5**:e15655.
- 135 Ekpenyong, A. E., Whyte, G., Chalut, K., Pagliara, S., Lautenschlager, F., Fiddler, C., Paschke, S., Keyser, U. F., Chilvers, E. R. & Guck, J. Viscoelastic Properties of Differentiating Blood Cells Are Fate- and Function-Dependent. *Plos One* 2012;7:e45237.
- 136 Gonzalez-Cruz, R. D., Fonseca, V. C. & Darling, E. M. Cellular mechanical properties reflect the differentiation potential of adipose-derived mesenchymal stem cells. *P Natl Acad Sci USA* 2012;**109**:E1523-E1529.
- 137 Bongiorno, T., Kazlow, J., Mezencev, R., Griffiths, S., Olivares-Navarrete, R., McDonald, J. E., Schwartz, Z., Boyan, B. D., McDevitt, T. C. & Sulchek, T. Mechanical stiffness as an improved single-cell indicator of osteoblastic human mesenchymal stem cell differentiation. *Journal of Biomechanics* 2014;47:2197-2204.
- 138 Lowry, W. E. & Quan, W. L. Roadblocks en route to the clinical application of induced pluripotent stem cells. *Journal of Cell Science* 2010;**123**:643-651.
- 139 Werbowetski-Ogilvie, T. E., Bosse, M., Stewart, M., Schnerch, A., Ramos-Mejia, V., Rouleau, A., Wynder, T., Smith, M. J., Dingwall, S., Carter, T., Williams, C., Harris, C., Dolling, J., Wynder, C., Boreham, D. & Bhatia, M. Characterization of human embryonic stem cells with features of neoplastic progression. *Nat Biotechnol* 2009;**27**:91-97.
- 140 Reisman, M. & Adams, K. T. Stem cell therapy: a look at current research, regulations, and remaining hurdles. *P T* 2014;**39**:846-857.
- 141 Liu, Z., Lee, S. J., Park, S., Konstantopoulos, K., Glunde, K., Chen, Y. & Barman, I. Cancer cells display increased migration and deformability in pace with metastatic progression. *FASEB J* 2020;**34**:9307-9315.
- 142 Hong, S. & Krafft, A. E. Primary effusion lymphoma with herpesvirus 8 DNA in patients coinfected with HIV and hepatitis C virus: a report of 2 cases. *AIDS Read* 2001;**11**:418-

- 143 Mach, A. J., Adeyiga, O. B. & Di Carlo, D. Microfluidic sample preparation for diagnostic cytopathology. *Lab on a Chip* 2013;**13**:1011-1026.
- 144 Sahn, S. A. The value of pleural fluid analysis. *Am J Med Sci* 2008;**335**:7-15.
- 145 Renshaw, A. A. Reporting risk of malignancy/dysplasia in cytology: a potential way to improve communication, if not reputation. *Cancer* 2007;**111**:465-466.
- 146 Yu, W., Lu, Q.-Y., Sharma, S., Ly, C., Di Carlo, D., Rowat, A. C., LeClaire, M., Kim, D., Chow, C., Gimzewski, J. K. & Rao, J. Single Cell Mechanotype and Associated Molecular Changes in Urothelial Cell Transformation and Progression. *Frontiers in Cell and Developmental Biology* 2020;8:601376.
- 147 Tse, H. T., Gossett, D. R., Moon, Y. S., Masaeli, M., Sohsman, M., Ying, Y., Mislick, K., Adams, R. P., Rao, J. & Di Carlo, D. Quantitative diagnosis of malignant pleural effusions by single-cell mechanophenotyping. *Sci Transl Med* 2013;**5**:1-9.
- 148 Remmerbach, T. W., Wottawah, F., Dietrich, J., Lincoln, B., Wittekind, C. & Guck, J. Oral cancer diagnosis by mechanical phenotyping. *Cancer Res* 2009;**69**:1728-1732.
- 149 Jordan, M. A. & Wilson, L. Microtubules and actin filaments: dynamic targets for cancer chemotherapy. *Current opinion in cell biology* 1998;**10**:123-130.
- 150 Kavallaris, M. Microtubules and resistance to tubulin-binding agents. *Nature Reviews Cancer* 2010;**10**:194-204.
- 151 LORIA, P., MILLER, S., FOLEY, M. & TILLEY, L. Inhibition of the peroxidative degradation of haem as the basis of action of chloroquine and other quinoline antimalarials. *Biochemical Journal* 1999;**339**:363-370.
- 152 Deng, X., Duffy, S. P., Myrand-Lapierre, M.-E., Matthews, K., Santoso, A. T., Du, Y.-L., Ryan, K. S. & Ma, H. Reduced deformability of parasitized red blood cells as a biomarker for anti-malarial drug efficacy. *Malaria journal* 2015;14:428.
- 153 Schilsky, R. L. Personalized medicine in oncology: the future is now. *Nature reviews Drug discovery* 2010;**9**:363-366.
- 154 Shapiro, H. M. Practical flow cytometry. 4th edn, (Wiley-Liss, 2003).
- 155 Choi, G., Murphy, E. & Guan, W. H. Microfluidic Time-Division Multiplexing Accessing Resistive Pulse Sensor for Particle Analysis. *Acs Sensors* 2019;**4**:1957-1963.
- 156 Liu, R. X., Wang, N. Q., Kamili, F. & Sarioglu, A. F. Microfluidic CODES: a scalable multiplexed electronic sensor for orthogonal detection of particles in microfluidic channels. *Lab on a Chip* 2016;**16**:1350-1357.

- 157 Uva, P., Cossu-Rocca, P., Loi, F., Pira, G., Murgia, L., Orru, S., Floris, M., Muroni, M. R., Sanges, F., Carru, C., Angius, A. & De Miglio, M. R. miRNA-135b Contributes to Triple Negative Breast Cancer Molecular Heterogeneity: Different Expression Profile in Basal-like Versus non-Basal-like Phenotypes. *Int J Med Sci* 2018;**15**:536-548.
- 158 Hourigan, C. S., Gale, R. P., Gormley, N. J., Ossenkoppele, G. J. & Walter, R. B. Measurable residual disease testing in acute myeloid leukaemia. *Leukemia* 2017;**31**:1482-1490.
- 159 Hallow, D. M., Seeger, R. A., Kamaev, P. P., Prado, G. R., LaPlaca, M. C. & Prausnitz, M. R. Shear-induced intracellular loading of cells with molecules by controlled microfluidics. *Biotechnol Bioeng* 2008;**99**:846-854.
- 160 Sharei, A., Zoldan, J., Adamo, A., Sim, W. Y., Cho, N., Jackson, E., Mao, S., Schneider, S., Han, M. J., Lytton-Jean, A., Basto, P. A., Jhunjhunwala, S., Lee, J., Heller, D. A., Kang, J. W., Hartoularos, G. C., Kim, K. S., Anderson, D. G., Langer, R. & Jensen, K. F. A vector-free microfluidic platform for intracellular delivery. *P Natl Acad Sci USA* 2013;110:2082-2087.
- 161 Heisenberg, C. P. & Bellaiche, Y. Forces in Tissue Morphogenesis and Patterning. *Cell* 2013;**153**:948-962.